Citation for published version:
Qu, X, Allan, A, Chui, G, Hutchings, TJ, Jiao, P, Johnson, L, Leung, WY, Li, PK, Steel, GR, Thompson, AS, Threadgill, MD, Woodman, TJ & Lloyd, MD 2013, 'Hydrolysis of ibuprofenoyl-CoA and other 2-APA-CoA esters by human acyl-CoA thioesterases-1 and -2 and their possible role in the chiral inversion of profens', Biochemical Pharmacology, vol. 86, no. 11, pp. 1621-1625. https://doi.org/10.1016/j.bcp.2013.08.067

DOI:
10.1016/j.bcp.2013.08.067

Publication date:
2013

Document Version
Peer reviewed version

Link to publication

Graphical Abstract

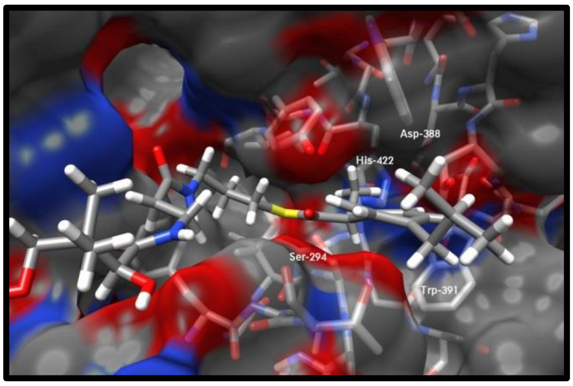

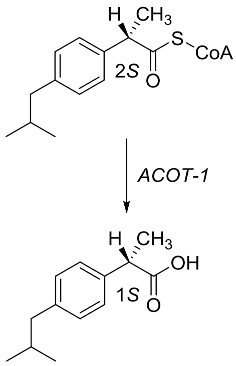

Acyl-CoA thioesterase-1 and -2 catalyse hydrolysis of 2-APA-CoA esters. The results suggest ACOT-1 plays a key role in the chiral inversion of ibuprofen and other 2-APA drugs.

Hydrolysis of ibuprofenoyl-CoA and other 2-APA-CoA esters by human acyl-CoA thioesterases-1 and -2 and their possible role in the chiral inversion of profens.

Xiao Qu, Amanda Allan, Grace Chui, Thomas J. Hutchings, Ping Jiao, Lawrence Johnson, Wai Y. Leung, Portia K. Li, Georgina R. Steel, Andrew S. Thompson, Michael D. Threadgill, Timothy J. Woodman, and Matthew D. Lloyd*

Medicinal Chemistry, Department of Pharmacy & Pharmacology, University of Bath, Claverton Down, Bath BA2 7AY, U. K.

*Author for correspondence: M.D.Lloyd@bath.ac.uk

Keywords: Acyl-CoA thioesterase (ACOT); Ibuprofen; Branched-chain fatty acids; α-Methylacyl-CoA racemase (AMACR; P504S); NSAID.

Abbreviations used: ACOT, acyl-CoA thioesterase; BSA, bovine serum albumin; DTNB, 5,5′-Dithiobis(2-nitrobenzoic acid); HEPES, 4-(2-Hydroxyethyl)piperazine-1-ethanesulfonic acid, NSAIDs, non-steroidal anti-inflammatory drugs; PMSF, phenylmethylsulfonyl fluoride; SDS-PAGE, sodium dodecyl sulfate polyacrylamide gel electrophoresis.

Abstract

Ibuprofen and related 2-arylpropanoic acid (2-APA) drugs are often given as a racemic mixture and the *R*-enantiomers undergo activation *in vivo* by metabolic chiral inversion. The chiral inversion pathway consists of conversion of the drug to the coenzyme A ester (by an acyl-CoA synthetase) followed by chiral inversion by α-methylacyl-CoA racemase (AMACR; P504S). The enzymes responsible for hydrolysis of the product *S*-2-APA-CoA ester to the active *S*-2-APA drug have not been identified. In this study, conversion of a variety of 2-APA-CoA esters by human acyl-CoA thioesterase-1 and -2 (ACOT-1 and -2) was investigated. Human recombinant ACOT-1 and -2 (ACOT-1 and -2) were both able to efficiently hydrolyse a variety of 2-APA-CoA substrates. Studies with the model substrates *R*- and *S*-2-methylmyristoyl-CoA showed that both enzymes were able to efficiently hydrolyse both of the epimeric substrates with (2*R*)- and (2*S*)- methyl groups. ACOT-1 is located in the cytosol and is able to hydrolyse 2-APA-CoA esters exported from the mitochondria and peroxisomes for inhibition of cyclo-oxygenase-1 and -2 in the endoplasmic reticulum. It is a prime candidate to be the enzyme responsible for the pharmacological action of chiral inverted drugs. ACOT-2 activity may be important in 2-APA toxicity effects and for the regulation of mitochondrial free coenzyme A levels. These results support the idea that 2-APA drugs undergo chiral inversion *via* a common pathway.

1. Introduction

Non-steroidal anti-inflammatory drugs (NSAIDs) are widely used in both human and veterinary medicine. Important examples of NSAIDs include aspirin, indomethacin, diclofenac and ibuprofen. Ibuprofen is a member of the 2-arylpropanoic acid (2-APA; a.k.a. profens) group of drugs, and it is probably the most widely used non-prescription drug. The accepted pharmacological targets of ibuprofen, cyclo-oxygenases-1 and -2 (COX-1 and -2), are potently inhibited by its *S*-enantiomer, whilst the *R*-enantiomer is much less effective [1]. *In vivo* the *R*-enantiomer of ibuprofen undergoes rapid uni-directional conversion into the *S*-enantiomer [2, 3], a metabolic process known as chiral inversion. Consequently, *R*-ibuprofen is activated as an inhibitor of COX-1 and -2.

The chiral inversion pathway (Figure 1) consists of three phases: 1) Stereoselective conversion of the *R*-ibuprofen **1*R*** to *R*-ibuprofenoyl-CoA **2*R*** by long-chain acyl-CoA synthetase [4-6] *via* an acyl-adenylate intermediate [7]; 2) Conversion of the *R*-ibuprofenoyl-CoA **2*R*** into a *ca.* 1:1 mixture of *R*- and *S*-ibuprofenoyl-CoA **2*R*/2*S*** by α-methylacyl-CoA racemase [8-10] (ibuprofenoyl-CoA epimerase [11, 12]); and 3) Hydrolysis of both ibuprofenoyl-CoA epimers **2** [13] to a racemic mixture of ibuprofen **1** by an undefined acyl-CoA thioesterase (ACOT). Product *R*-ibuprofen **1*R*** is reconverted back to its acyl-CoA ester, whilst *S*-ibuprofen **1*S*** is not recycled and this accounts for the overall uni-directional $R \rightarrow S$ chiral inversion of the pathway. Most other 2-APA drugs also undergo *in vivo* chiral inversion in humans (reviewed in [8]), and α-methylacyl-CoA racemase has been shown to accept several other 2-APA-CoA esters as substrates [9].

Microsomal [14] long-chain fatty acyl-CoA synthetase (ibuprofenoyl-CoA synthetase [4]) produces *R*-2-APA-CoA esters which are imported into mitochondria and peroxisomes (probably via the acyl-carnitine shuttle [15]), for chiral inversion by α-methylacyl-CoA racemase [16-18]. Cyclo-oxygenase-1 and -2 (a.k.a. prostaglandin E2 synthetase or endoperoxidase) [1, 19] are located in the endoplasmic reticulum [20, 21], implying that *S*-2-APA-CoA esters must be exported (via a reverse carnitine shuttle [22]) to interact with the target. Hydrolysis of 2-APA-CoA esters within mitochondria has also been linked to 2-APA toxicity [23, 24]. Humans contain a large number of ACOT enzymes [25-27], with ACOT-1 localised in the cytosol and ACOT-2 localised in mitochondria [27]. This paper reports a study on the possible roles of human ACOT-1 and ACOT-2 in the 2-APA chiral inversion pathway.

2. Materials and Methods

2.1. Sources of materials:

All chemicals were obtained from the Sigma-Aldrich Chemical Co. or Fisher Scientific Ltd and were used without further purification, unless otherwise noted. Aqueous solutions were made in 18.2 Mega-Ω.cm Milli-Q water and pH adjusted with HCl or NaOH solutions as appropriate. KOD polymerase, the pET46 vector system, competent cells, Bugbuster, and Benzonase were obtained from Novagen. IPTG was from Calbiochem. Dpn1 was from New England Biolabs. Primers and protein molecular weight markers were from Invitrogen. Plasmids were obtained from imaGenes Gmbh, Germany (http://www.lifesciences.sourcebioscience.com/; ACOT-1: IRCMp5012A0824D; Hs.568046; ACOT-2: IRAUp969B0534D; Hs.649479). The syntheses of myristoyl-CoA **3** and *R*- and *S*-2-methylmyristoyl-CoA, **4*R*** and **4*S***, are described in Supplementary Information available from the corresponding author. ±-Fenoprofenoyl-CoA **5**, ±-flurbiprofenoyl-CoA **6**, ±-ibuprofenoyl-CoA **2**, *S*-ketoprofenoyl-CoA **11** and *S*-naproxenoyl-CoA **12** were synthesised as previously described [9].

2.3. Sub-cloning of human ACOT-1 and -2:

ACOT-1 was amplified using the following primers: *forward*, GACGACGACAAGATGGCGGCGACGCTGAT; *reverse*, GAGGAGAAGCCCGGTTACACTTTTGATGGGATTGTCCC. ACOT-2 was amplified using the following primers: *forward*, GACGACGACAAGATGTCTAACAAGCTTCTTTCTCCCCA; *reverse*, GAGGAGAAGCCCGGTTACACTTTTGATGGGATTGTCCC. PCR reactions contained the following: plasmid template (1 μL; 100 ng); primers (2 x 3 μL; 5 μM each); buffer (5 μL); dNTPs (5 μL); $MgSO_4$ (2 μL); KOD polymerase (1 μL, 2.5 activity units); and sterile water (30 μL). Reactions were amplified by the following procedure: 94 ºC, 2 min; 35 cycles of: 94 ºC, 15 s; 52 ºC, 30s; 68 ºC, 2 min; followed by 72 ºC, 2 min. The reaction products were treated with dpn1 (2 μL, 40 activity units) for 2 h at 37 ºC to remove template DNA, and the presence of the amplified DNA confirmed by 1% agarose gel electrophoresis. The PCR product was purified using a QIAquick PCR purification kit (Qiagen) and quantified (GeneQuant). The product was inserted into the pET46 vector according to the manufacturers' instructions and transformed into Giga cells. Single colonies were selected, grown in 5 mL Lennox LB media supplemented with ampicillin (50 μg/mL) and plasmids prepared. The presence of the required insert in the plasmid was confirmed by PCR analysis using 1 μL template in a final volume of 20 μL followed by 1% (w/v) agarose gel electrophoresis. DNA sequencing confirmed the sequence of ACOT-1 was identical to A1L172 (http://www.uniprot.org). The sequence of ACOT-2 was identical to P49753 with the known A454V polymorphism.

2.4. Expression and purification of ACOT enzymes

Expression plasmids were transformed into *E. coli* BL21 (DE3) pLysS [28] and grown in Lennox LB media supplemented with ampicillin (50 μg/mL) and chloramphenicol (32 μg/mL) at 37 ºC and 190 r.p.m. Starter culture (30 mL) was used to inoculate 1L of the same media, grown under the same conditions until OD_{600} = ~1.5 and induced with 1 mM IPTG. Cells were harvested after 3 hours by centrifugation (JA-10 rotor, 9,000 r.p.m., 14 300 *g*, 20 min., 4 ºC) and stored at -80 ºC.

Cells (*ca.* 5 g) were lysed using 30 mL Bugbuster supplemented with 250 u Benzonase at 4 ºC, followed by centrifugation [28]. The crude extract was filtered and loaded onto a 5 mL HisTrap FF Ni^{2+} column equilibrated in 20 mM NaH_2PO_4-NaOH, 300 mM NaCl, 10 mM imidazole, pH 7.2. The column was washed with 10 mL buffer and eluted with 300 mM imidazole-HCl, pH 7.2 in the same buffer. Fractions (5 mL) were analysed by 10% SDS-PAGE, and those containing ACOTs were pooled and dialysed against 20 mM HEPES-NaOH, pH 7.27 (3 x 650 mL). Protein concentrations were determined using absorbance at 280 nm with parameters calculated with protparam (http://web.expasy.org/protparam/) for the His-tag enzyme: ACOT-1; M_w = 48 009.1 Da., ε_{280} = 48 360 M^{-1} cm^{-1}; ACOT-2; M_w = 54 978.3 Da., ε_{280} = 55 350 M^{-1} cm^{-1}.

2.5. ACOT assays

Assays were conducted in 50 mM HEPES-NaOH, pH 7.27 in a final volume of 100 μL at 25 ºC. Rates at each substrate concentration were measured using three dependent repeats. Reactions were carried out at pH 7.27, as this minimizes spontaneous hydrolysis of DTNB [29]. Assay mixtures contained substrate at the required concentration, DTNB (100 μM) and enzyme (50-75 μg). Myristoyl-CoA **3** and *R*- and *S*-2-methylmyristoyl-CoA (***4R*** and ***4S***) were pre-incubated with BSA at a constant ratio [substrate: BSA (100: 2.88 μM)] for 10 minutes before assaying. Assays using 2-APA-CoA substrates did not contain BSA. Reaction rates were obtained by plotting changes in absorbance with Excel. Activities in $nmol.min.^{-1}mg^{-1}$ were calculated assuming ε_{412} = 14.15 mM^{-1} cm^{-1} at 25 ºC [29, 30], and kinetic parameters obtained using the Direct Linear Plot [31, 32] in SigmaPlot 11 and enzyme kinetics module 1.3. Kinetic plots for all substrates are available in Supplementary Information, available from the corresponding author.

2.6. Structural models of ACOT-2

Models were produced based on the X-ray crystal structure of human ACOT-2 determined without any substrate [32]. The binding pocket was identified based on the proximity to the active site residues Ser-294, Asp-388 and His-422. Once docked, the 2-APA-CoAs were subjected to molecular mechanics and dynamics calculations to establish optimal docking conformations; during these calculations, the enzyme and coenzyme A moiety were restrained to original conformations. The 2-APA-CoA and binding pocket were subjected to molecular dynamics and finally molecular mechanics calculations to give the final structures. Calculations were performed using the Tripos Associates force fields within the SYBYL-X 2.0 software suite on a dual Intel quad core workstation (Windows 7). Gasteiger-Hückel charges were calculated and used within the complexes.

3. Results

Recombinant human ACOT-1 and ACOT-2 were produced with an N-terminal His-tag sequence and purified by metal-chelate chromatography. The 2-APA-CoA esters which had previously been shown to be substrates for α-methylacyl-CoA racemase [9] were synthesised for testing as substrates (Figure 2). *R*- and *S*-2-methylmyristoyl-CoA (**4*R*** and **4*S***) were synthesised by modification of the route for *R*- and *S*-2-methyldecanoyl-CoA [33] to investigate the effect of the 2-methyl group epimeric configuration on substrate conversion. Myristoyl-CoA **3** was synthesised as a known good substrate of ACOT-1 and ACOT-2 [28].

The conversion of acyl-CoA esters to their corresponding acids and reduced coenzyme A by ACOT-1 and -2 was assessed using the reported assay with DTNB [28]. All of the tested acyl-CoA esters were efficiently converted to products (Tables 1 and 2). Myristoyl-CoA **3**, *R*-2-methylmyristoyl-CoA **4*R*** and *S*-2-methylmyristoyl-CoA **4*S*** showed Michaelis-Menten behaviour as substrates for ACOT-1 and ACOT-2. In the case of ACOT-1 (Table 1) a K_m value of 39 μM was determined for myristoyl-CoA **3**, compared to 9.3 and 12 μM for 2-methylmyristoyl-CoA **4*R*** and **4*S***, respectively. Catalytic efficiency (as measured by k_{cat}/K_m) was determined to be 151 M^{-1} s^{-1} for myristoyl-CoA **3**, 128 M^{-1} s^{-1} for *R*-2-methylmyristoyl-CoA **4*R*** and 230 M^{-1} s^{-1} for *S*-2-methylmyristoyl-CoA **4*S***, showing that the 2*S*- substrate was somewhat preferred. In the case of ACOT-2 (Table 2), *R*-2-methylmyristoyl-CoA **4*R*** was converted most efficiently (as judged by k_{cat}/K_m), followed by myristoyl-CoA **3** and *S*-2-methylmyristoyl-CoA **4*S***. Thus, both ACOT enzymes show some preference for particular epimeric configurations of the 2-methylmyristoyl-CoA substrate **4**.

Hydrolysis of 2-APA-CoA esters to their corresponding acids by ACOT-1 and ACOT-2 was then investigated, and all of the tested 2-APA-CoAs were good substrates (Tables 1 & 2) and proper Michaelis-Menten kinetics were observed. In the case of ACOT-1 (Table 1) most substrates, including ibuprofenoyl-CoA (Figure 3), were converted with similar efficiencies (k_{cat}/K_m = 140-220 M^{-1} s^{-1}), except for *S*-ketoprofenoyl-CoA **7*S*** (k_{cat}/K_m = 45 M^{-1} s^{-1}). This shows that ACOT-1 has a broad substrate selectivity. In the case of ACOT-2 (Table 2), the best 2-APA-CoA substrates were ±-fenoprofenoyl-CoA **5** and ±-flurbiprofenoyl-CoA **6** (k_{cat}/K_m = *ca.* 320 M^{-1} s^{-1}), followed by *S*-naproxenoyl-CoA **8** (k_{cat}/K_m = 249 M^{-1} s^{-1}), *S*-ketoprofenoyl-CoA **7** (k_{cat}/K_m = 145 M^{-1} s^{-1}) and ±-ibuprofenoyl-CoA **2** (k_{cat}/K_m = 70 M^{-1} s^{-1}). Thus, ACOT-2 showed a somewhat higher variability in substrate conversion efficiency, with the best substrates been converted somewhat more efficiently than by ACOT-1 (k_{cat}/K_m = 346 *cf* 230 s^{-1} M^{-1}).

The substrate selectivity of ACOT-1 and -2 was further investigated by a substrate docking study (Figure 4) starting from the crystal structure of the ACOT-2 enzyme without any substrate bound [32]. ACOT-1 and ACOT-2 have almost identical core amino acid sequences, and hence are expected to possess similar substrate selectivities. The binding position of the acyl-CoA moiety was established by proximity to Ser-294, His-422 and Asp-388, the catalytic triad which performs the hydrolysis reaction. Two small pockets accommodate the methyl groups of 2*R*- and 2*S*- substrates, explaining how both epimers of 2-methyl substrates can be hydrolysed and the preference for branched-chain acyl-CoA esters over straight-chain acyl-CoA esters. The aromatic side-chain common to all 2-APA drugs projects into a deep lipophilic pocket, forming transient π stacking interactions with the side-chain of Trp-391. This lipophilic pocket also accommodates the various substituents on the aromatic ring in the various 2-APA drugs. The phosphopantetheinyl- side-chain of the CoA moiety is enclosed within a narrow tunnel lined with acidic and basic residues. Several possible sites were available for the 3-phospho-adenosine moiety, and modelling studies proved inconclusive with multiple binding configurations with similar energies observed.

4. Discussion

Humans contain a large number of ACOT enzymes [25-28, 34], and ACOTs -1, -2, -4 and -8 were identified as potentially been able to hydrolyse substrates possessing 2-methyl groups based on previous work. ACOT-1 was selected for further study since it was potentially able to hydrolyse inverted 2-APA-CoA esters exported from mitochondria and peroxisomes into the cytosol. ACOT-2 was also selected for further study as it is localised in mitochondria, and can potentially hydrolyse 2-APA-CoA esters imported via the acyl-carnitine shuttle and hence potentially contribute to 2-APA-mediated toxicity mechanisms [23]. ACOT-1 and ACOT-2 are both type I enzymes and share very high sequence identity within their core regions [34]; ACOT-2 mainly differs in that it possesses a N-terminal mitochondrial targeting signal which is absent in ACOT-1 (Supplementary Information, Figure S1).

Both ACOT-1 and ACOT-2 show limited discrimination between different chiral configurations of the substrate, as demonstrated by conversion of both *R*- and *S*-2-methylmyristoyl-CoA (**4*R*** and **4*S***). The results are consistent with the previous observations that both epimers of ibuprofenoyl-CoA [13] and fenoprofenoyl-CoA [35] can be hydrolysed in the chiral inversion pathway. The broad substrate selectivity of ACOT-1 and ACOT-2 is similar to that observed for α-methylacyl-CoA racemase [9], and is consistent with a common chiral inversion pathway existing for all 2-APA drugs undergoing chiral inversion. The observed uni-directional $R \rightarrow S$ chiral inversion *in vivo* is due to stereoselective formation of *R*-2-APA-CoA esters by long-chain fatty acyl-CoA synthetase [4-6]. *R*-Flurbiprofen does not undergo chiral inversion in humans, although it does in other mammalian species [36, 37], despite ±-flurbiprofenoyl-CoA **6** been a substrate for both AMACR [9] and ACOTs. Studies on purified long-chain fatty acyl-CoA synthetase [4] have shown that *R*-

Flurbiprofen is not converted to *R*-flurbiprofenoyl-CoA **6*R***. It therefore seems likely that the failure of flurbiprofen to undergo chiral inversion in humans is due to non-formation of the acyl-CoA ester *in vivo* [8, 9].

The results in this paper show that both ACOT-1 and ACOT-2 possess broad substrate selectivity. Modelling studies (Figure 4) support the roles of the proposed catalytic residues [38] and explain how the enzyme is able to accommodate straight-chain and both epimeric configurations of 2-methyl substrates. Branched-chain substrates are slightly preferred (based on k_{cat}/K_m values), presumably due to accommodation of the 2-methyl group within their binding pockets and this is consistent with other enzymes that metabolise branched-chain acyl-CoA substrates [39]. The π stacking interactions with the side-chain of Trp-391 explains the favourable binding of 2-APA-CoA esters, and the lipophilic binding pocket the tolerance for diverse side-chain structures. The situation is reminiscent of that observed for AMACR [9], the enzyme catalysing the chiral inversion step in the metabolic pathway, in which broad substrate selectivity is achieved by non-specific hydrophobic interactions with a methionine-rich surface. Some 2-APA-CoA substrates are converted much less efficiently by ACOT-1 or ACOT-2 than most substrates, most notably *S*-ketoprofenoyl-CoA **7*S*** (ACOT-1) and ±-ibuprofenoyl-CoA **2** (ACOT-2). The reasons why these substrates are converted less efficiently are unclear.

In summary, 2-APA-CoA esters are good substrates for both ACOT-1 and ACOT-2. These enzymes appear to play a central role in the chiral inversion pathway of 2-APA drugs, catalysing the third step in the pathway. The results also support a common chiral inversion pathway for all 2-APA drugs.

Acknowledgements

Parts of this work were carried out as a Nuffield Undergraduate Research Bursary, Nuffield Science Bursaries for Schools and Colleges, a Bath-Shangdong Pharmacy & Pharmacology Exchange

Project and a Masters in Pharmacy final year project at the University of Bath. AST, MDT, TJW and MDL are members of the Cancer Research @ Bath network.

References

[1] Mitchell JA, Akarasereenont P, Thiemermann C, Flower RJ, Vane JR. Selectivity of nonsteroidal antiinflammatory drugs as inhibitors of constituative and inducible cyclooxygenase. Proc Natl Acad Sci USA 1993;90:11693-7.

[2] Wechter WJ, Loughhead DG, Reischer RJ, Vangiessen GJ, Kaiser DG. Enzymatic inversion at saturated carbon - Nature and mechanism of inversion of *R*(-) *p-iso*-butyl hydratropic acid. Biochem Biophys Res Commun 1974;61:833-7.

[3] Nakamura Y, Yamaguchi T, Takahashi S, Hashimoto S, Iwantani K, Nakagawa Y. Optical isomerization mechanism of *R*(-)-hydratropic acid derivatives. 12th Symposium on Drug Metabolism and Action. Kanazawa: Pharmaceutical Society of Japan, 1980. p. s-1.

[4] Brugger R, Reichel C, Alia BG, Brune K, Yamamoto T, Tegeder I, et al. Expression of rat liver long-chain acyl-CoA synthetase and characterization of its role in the metabolism of *R*-ibuprofen and other fatty acid-like xenobiotics. Biochem Pharmacol 2001;61:651-6.

[5] Brugger R, Alia BG, Reichel C, Waibel R, Menzel S, Brune K, et al. Isolation and characterization of rat liver microsomal *R*-ibuprofenoyl-CoA synthetase. Biochem Pharmacol 1996;52:1007-13.

[6] Sevoz C, Benoît E, Buronfosse T. Thioesterification of 2-arylpropionic acids by recombinant acyl-coenzyme A synthetases (ACS1 and ACS2). Drug Metab Disposit 2000;28:398-402.

[7] Menzel S, Waibel R, Brune K, Geisslinger G. Is the formation of *R*-ibuprofenoyl-adenylate the first stereoselective step of chiral inversion? Biochem Pharmacol 1994;48:1056-8.

[8] Lloyd MD, Yevglevskis M, Lee GL, Wood PJ, Threadgill MD, Woodman TJ. α-Methylacyl-CoA racemase (AMACR): Metabolic enzyme, drug metabolizer and cancer marker P504S. Prog Lipid Res 2013;52:220-30.

[9] Woodman TJ, Wood PJ, Thompson AS, Hutchings TJ, Steel GR, Jiao P, et al. Chiral inversion of 2-arylpropionyl-CoA esters by α-methylacyl-CoA racemase 1A (AMACR; P504S). Chem Commun 2011;47:7332-4.

[10] Lloyd MD, Darley DJ, Wierzbicki AS, Threadgill MD. α-Methylacyl-CoA racemase: An 'obscure' metabolic enzyme takes centre stage. FEBS J 2008;275:1089-102.

[11] Shieh WR, Chen CS. Purification and characterization of novel 2-arylpropionyl-CoA epimerases from rat-liver cytosol and mitochondria. J Biol Chem 1993;268:3487-93.

[12] Reichel C, Brugger R, Bang H, Geisslinger G, Brune K. Molecular cloning and expression of a 2-arylpropionyl-coenzyme A epimerase: A key enzyme in the inversion metabolism of ibuprofen. Mol Pharmacol 1997;51:576-82.

[13] Knihinicki RD, Day RO, Williams KM. Chiral Inversion of 2-arylpropionic acid nonsteroidal antiinflammatory drugs. 2. Racemization and hydrolysis of (*R*)-ibuprofen-CoA and (*S*)-ibuprofen-CoA thioesters. Biochem Pharmacol 1991;42:1905-11.

[14] Watkins PA, Howard AE, Gould SJ, Avigan J, Mihalik SJ. Phytanic acid activation in rat liver peroxisomes is catalyzed by long-chain acyl-CoA synthetase. J Lipid Res 1996;37:2288-95.

[15] Visser WF, van Roermund CWT, Ijlst L, Waterham HR, Wanders RJA. Metabolite transport across the peroxisomal membrane. Biochem J 2007;401:365-75.

[16] Amery L, Fransen M, De Nys K, Mannaerts GP, Van Veldhoven PP. Mitochondrial and peroxisomal targeting of 2-methylacyl-CoA racemase in humans. J Lipid Res 2000;41:1752-9.

[17] Ferdinandusse S, Denis S, Ijlst L, Dacremont G, Waterham HR, Wanders RJA. Subcellular localization and physiological role of α-methylacyl-CoA racemase. J Lipid Res 2000;41:1890-6.

[18] Kotti TJ, Savolainen K, Helander HM, Yagi A, Novikov DK, Kalkkinen N, et al. In mouse α-methylacyl-CoA racemase, the same gene product is simultaneously located in mitochondria and peroxisomes. J Biol Chem 2000;275:20887-95.

[19] Smith WL, Urade Y, Jakobsson P-J. Enzymes of the cyclooxygenase pathways of prostanoid biosynthesis. Chem Rev 2011;111:5821-65.

[20] Spencer AG, Woods JW, Arakawa T, Singer, II, Smith WL. Subcellular localization of prostaglandin endoperoxide H synthases-1 and -2 by immunoelectron microscopy. J Biol Chem 1998;273:9886-93.

[21] Mukherjee E, Ghosh D. Sub-cellular localization of cyclo-oxygenase-prostaglandin-E2 synthetase complex in goat vesicular gland by catalytic activity analysis. Prostaglandins 1989;38:557-63.

[22] Ventura FV, Ijlst L, Ruiter J, Ofman R, Costa CG, Jakobs C, et al. Carnitine palmitoyltransferase II specificity towards β-oxidation intermediates - Evidence for a reverse carnitine cycle in mitochondria. Euro J Biochem 1998;253:614-8.

[23] Browne GS, Nelson C, Nguyen T, Ellis BA, Day RO, Williams KM. Stereoselective and substrate-dependent inhibition of hepatic mitochondrial β-oxidation and oxidative phosphorylation by the non-steroidal anti-inflammatory drugs ibuprofen, flurbiprofen, and ketorolac. Biochem Pharmacol 1999;57:837-44.

[24] Pessayre D, Mansouri A, Haouzi D, Fromenty B. Hepatotoxicity due to mitochondrial dysfunction. Cell Biol Toxicol 1999;15:367-73.

[25] Hunt MC, Siponen MI, Alexson SEH. The emerging role of acyl-CoA thioesterases and acyltransferases in regulating peroxisomal lipid metabolism. Biochim Biophys Acta 2012;1822:1397-410.

[26] Hunt MC, Alexson SEH. Novel functions of acyl-CoA thioesterases and acyltransferases as auxiliary enzymes in peroxisomal lipid metabolism. Prog Lipid Res 2008;47:405-21.

[27] Hunt MC, Yamada J, Maltais LJ, Wright MW, Podesta EJ, Alexson SEH. A revised nomenclature for mammalian acyl-CoA thioesterases/hydrolases. J Lipid Res 2005;46:2029-32.

[28] Hunt MC, Rautanen A, Westin MAK, Svensson LT, Alexson SEH. Analysis of the mouse and human acyl-CoA thioesterase (ACOT) gene clusters show that convergent, functional evolution results in a reduced number of human peroxisomal ACOTs. FASEB J 2006;20:1855-64.

[29] Riddles PW, Blakeley RL, Zerner B. Ellman's reagent - 5,5'dithiobis(2-nitrobenzoic acid) - re-examination. Anal Biochem 1979;94:75-81

[30] Eyer P, Worek F, Kiderlen D, Sinko G, Stuglin A, Simeon-Rudolf V, et al. Molar absorption coefficients for the reduced Ellman reagent: Reassessment. Anal Biochem 2003;312:224-7.

[31] Cornish-Bowden A, Eisenthal R. Statistical considerations in estimation of enzyme kinetic parameters by direct linear plot and other methods. Biochem J 1974;139:721-30.

[32] Eisenthal R, Cornish-Bowden A. Direct Linear Plot - New graphical method for estimating enzyme kinetic parameters. Biochem J 1974;139:715-20.

[33] Darley DJ, Butler DS, Prideaux SJ, Thornton TW, Wilson AD, Woodman TJ, et al. Synthesis and use of isotope-labelled substrates for a mechanistic study on human α-methylacyl-CoA racemase 1A (AMACR; P504S). Org Biomol Chem 2009;7:543-52.

[34] Kirkby B, Roman N, Kobe B, Kellie S, Forwood JK. Functional and structural properties of mammalian acyl-coenzyme A thioesterases. Prog Lipid Res 2010;49:366-77.

[35] Sevoz C, Rousselle C, Benoît E, Buronfosse T. *In vitro* study of fenoprofen chiral inversion in rat: comparison of brain *versus* liver. Xenobiotica 1999;29:1007-16.

[36] Leipold DD, Kantoci D, Murray Jr D, Quiggle DD, Wechter WJ. Bioinversion of *R*-flurbiprofen to *S*-flurbiprofen at various doses in rat, mouse, and monkey. Chirality 2004;16:379-87.

[37] Porubek DJ, Sanins SM, Stephens JR, Grillo MP, Kaiser DG, Halstead GW, et al. Metabolic chiral inversion of flurbiprofenoyl-CoA *in vitro*. Biochem Pharmacol 1991;42:R1-R4.

[38] Mandel CR, Tweel B, Tong L. Crystal structure of human mitochondrial acyl-CoA thioesterase (ACOT2). Biochem Biophys Res Commun 2009;385:630-3.

[39] Mukherji M, Kershaw NJ, Schofield CJ, Wierzbicki AS, Lloyd MD. Utilization of sterol carrier protein-2 by phytanoyl-CoA 2- hydroxylase in the peroxisomal α-oxidation of phytanic acid. Chem Biol 2002;9:597-605.

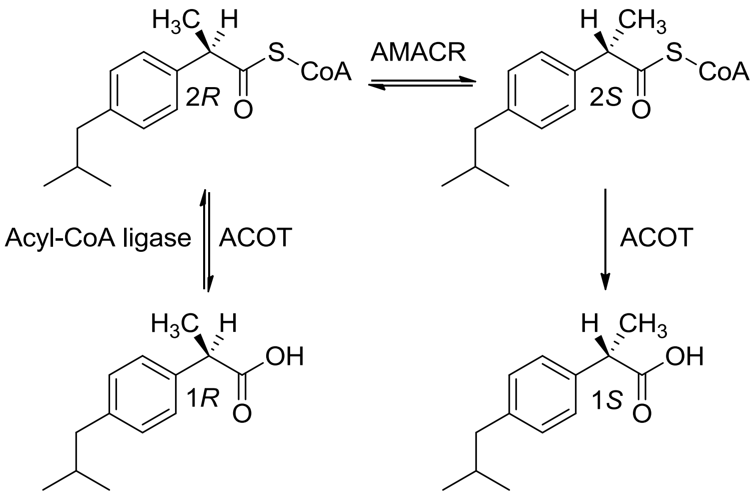

Figure 1: The chiral inversion pathway of 2-APA drugs, using ibuprofen **1** as an example.

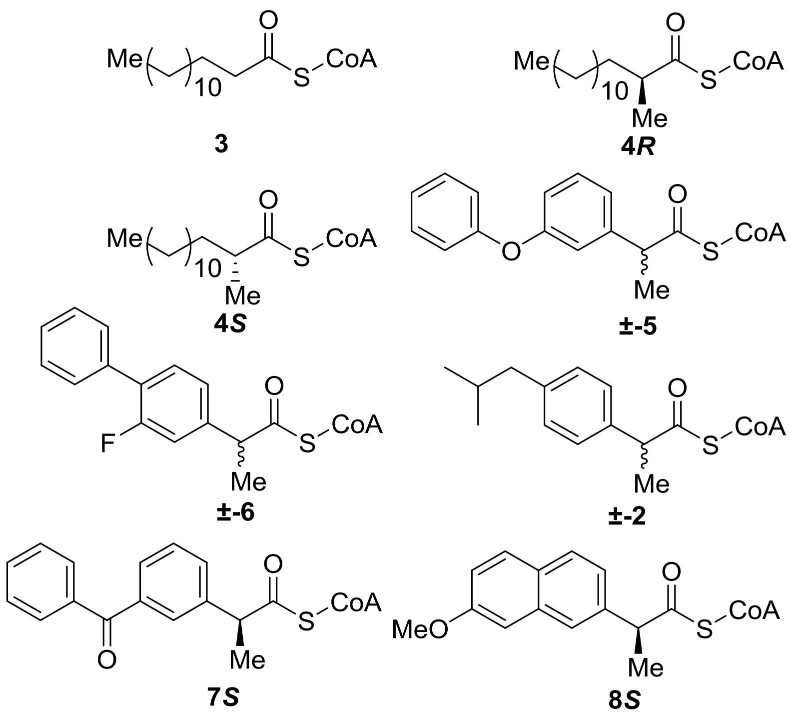

Figure 2: Acyl-CoA esters tested as substrates with human ACOT-1 and -2.

Substrate	K_m (μM)	V_{max} (nmol. min.$^{-1}$mg^{-1})	k_{cat} (s^{-1})	k_{cat}/K_m (s^{-1} M^{-1})
Myristoyl-CoA **3**	39	7.40	0.0059	151
R-2-Methylmyristoyl-CoA ***4R***	9.3	1.48	0.0012	128
S-2-Methylmyristoyl-CoA ***4S***	12	3.37	0.0027	230
±-Fenoprofenoyl-CoA **5**	32	6.89	0.0055	173
±-Flurbiprofenoyl-CoA **6**	18	5.07	0.0040	218
±-Ibuprofenoyl-CoA **2**	7.0	1.63	0.0013	186
S-Ketoprofenoyl-CoA ***7S***	11	0.62	0.0004	45
S-Naproxenoyl-CoA ***8S***	3.0	0.52	0.0004	141

Table 1: Kinetic parameters determined for human ACOT-1. Reported values are medians obtained from the Direct Linear Plot.

Substrate	K_m (μM)	V_{max} (nmol. min.$^{-1}$mg^{-1})	k_{cat} (s^{-1})	k_{cat}/K_m (s^{-1} M^{-1})
Myristoyl-CoA **3**	14.9	3.1	0.0028	192
R-2-Methylmyristoyl-CoA **4*R***	2.75	1.0	0.0009	346
S-2-Methylmyristoyl-CoA **4*S***	35.1	5.9	0.0054	155
±-Fenoprofenoyl-CoA **5**	21.2	7.5	0.0069	326
±-Flurbiprofenoyl-CoA **6**	25.5	8.7	0.0079	312
±-Ibuprofenoyl-CoA **2**	121	9.2	0.0084	70
S-Ketoprofenoyl-CoA **7*S***	3.65	0.57	0.0005	145
S-Naproxenoyl-CoA **8*S***	2.04	0.55	0.0005	249

Table 2: Kinetic parameters determined for human ACOT-2. Reported values are medians obtained from the Direct Linear Plot.

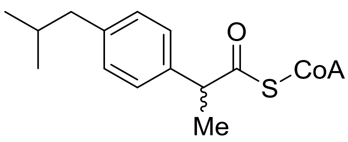

A.

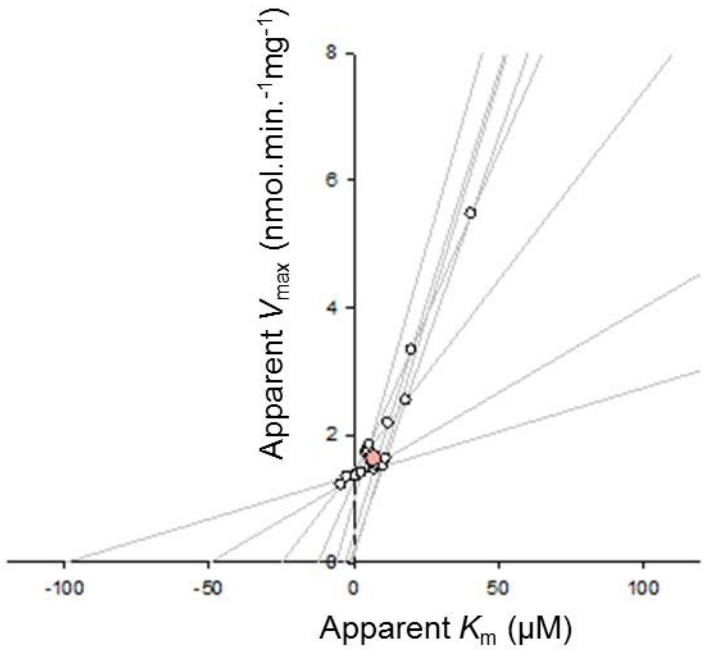

B.

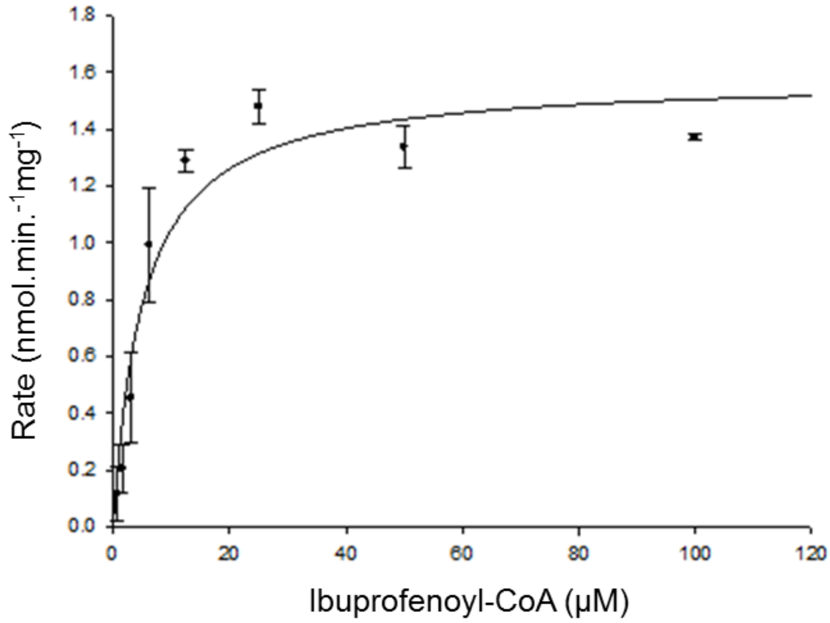

Figure 3: Kinetic plots of ibuprofenoyl-CoA hydrolysis catalysed by ACOT-1. A. Direct Linear Plot; B. Michaelis-Menten plot. Error bars are ± standard error (± SE).

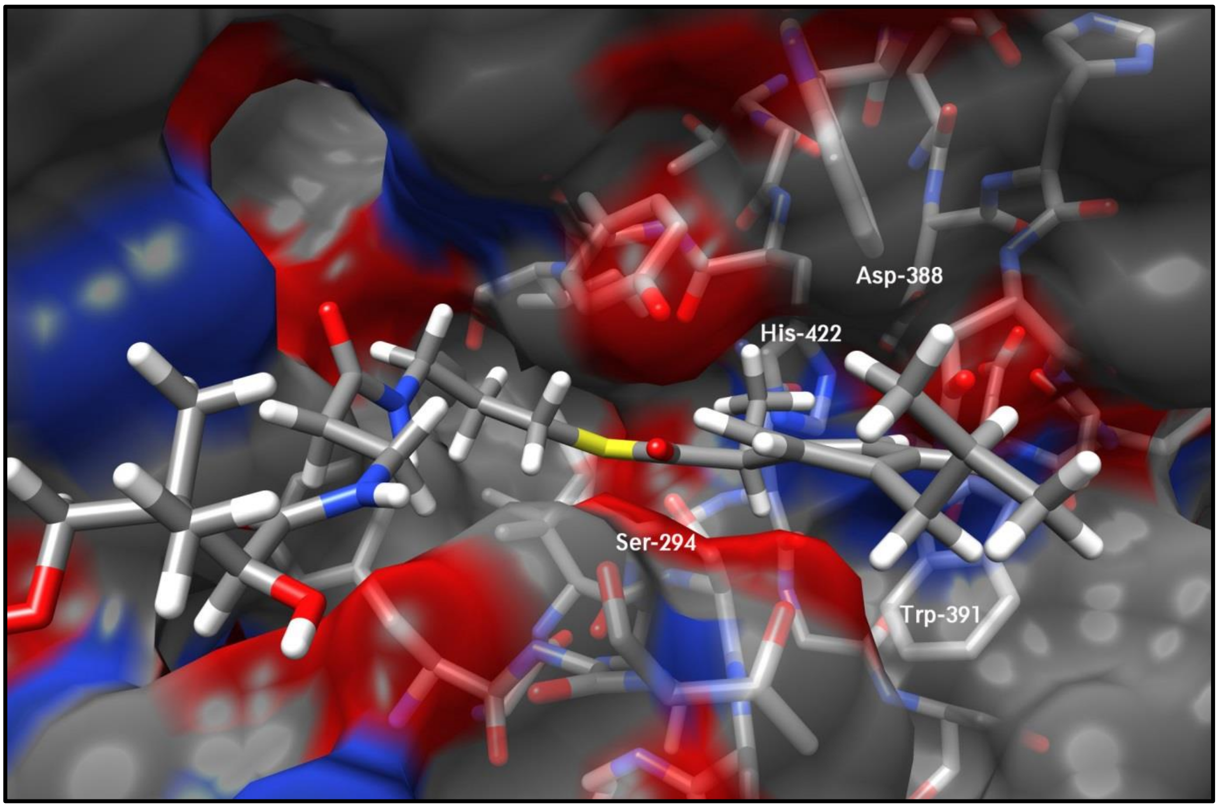

Figure 4: *S*-ibuprofenoyl-CoA bound into the ACOT2 binding pocket [32]. Ser-294 is located in the base of the pocket in close proximity to the carbonyl group of the thioester; His-422 and Asp-388 are located deeper within the enzyme. The exact orientation of the 3-phosphoadenosine moiety could not be established with several possible binding channels available.

Supplementary Information

Hydrolysis of ibuprofenoyl-CoA and other 2-APA-CoA esters by human acyl-CoA thioesterases-1 and -2 and their possible role in the chiral inversion of profens.

Xiao Qu, Amanda Allan, Grace Chui, Thomas J. Hutchings, Ping Jiao, Lawrence Johnson, Wai Y. Leung, Portia K. Li, Georgina R. Steel, Andrew S. Thompson, Michael D. Threadgill and Matthew D. Lloyd*

Medicinal Chemistry, Department of Pharmacy & Pharmacology, University of Bath, Claverton Down, Bath BA2 7AY, U. K.

*Author for correspondence: M.D.Lloyd@bath.ac.uk

Abbreviations used: ACOT, acyl-CoA thioesterase; BSA, bovine serum albumin; DTNB, 5,5′-Dithiobis(2-nitrobenzoic acid); HEPES, 4-(2-Hydroxyethyl)piperazine-1-ethanesulfonic acid, PMSF, phenylmethylsulfonyl fluoride; SDS-PAGE, sodium dodecyl sulfate polyacrylamide gel electrophoresis;

Table of Contents

Synthesis of substrates	pp. 3-7
Kinetic plots for ACOT-1 with 2-APA-CoA substrates	pp. 9-32
Kinetic plots for ACOT-2 with 2-APA-CoA substrates	pp. 33-56
Figure S1: Sequence alignment of human ACOT-1 and ACOT-2	p 57
References	p 58

Synthetic route to substrates

R-2-Methylmyristoyl-CoA **4*R*** and *S*-2-methylmyristoyl-CoA **4*S*** were synthesized by the same route as for *S*-2-methyldecanoyl-CoA and *R*-2-methyldecanoyl-CoA [40] (Scheme S1). Myristoyl-CoA **3** was synthesized by the reaction of myristic acid **9** (tetradecanoic acid) with carbonyl di-imidazole followed by coenzyme A. 2-APA-CoA esters were synthesized as previously described [9].

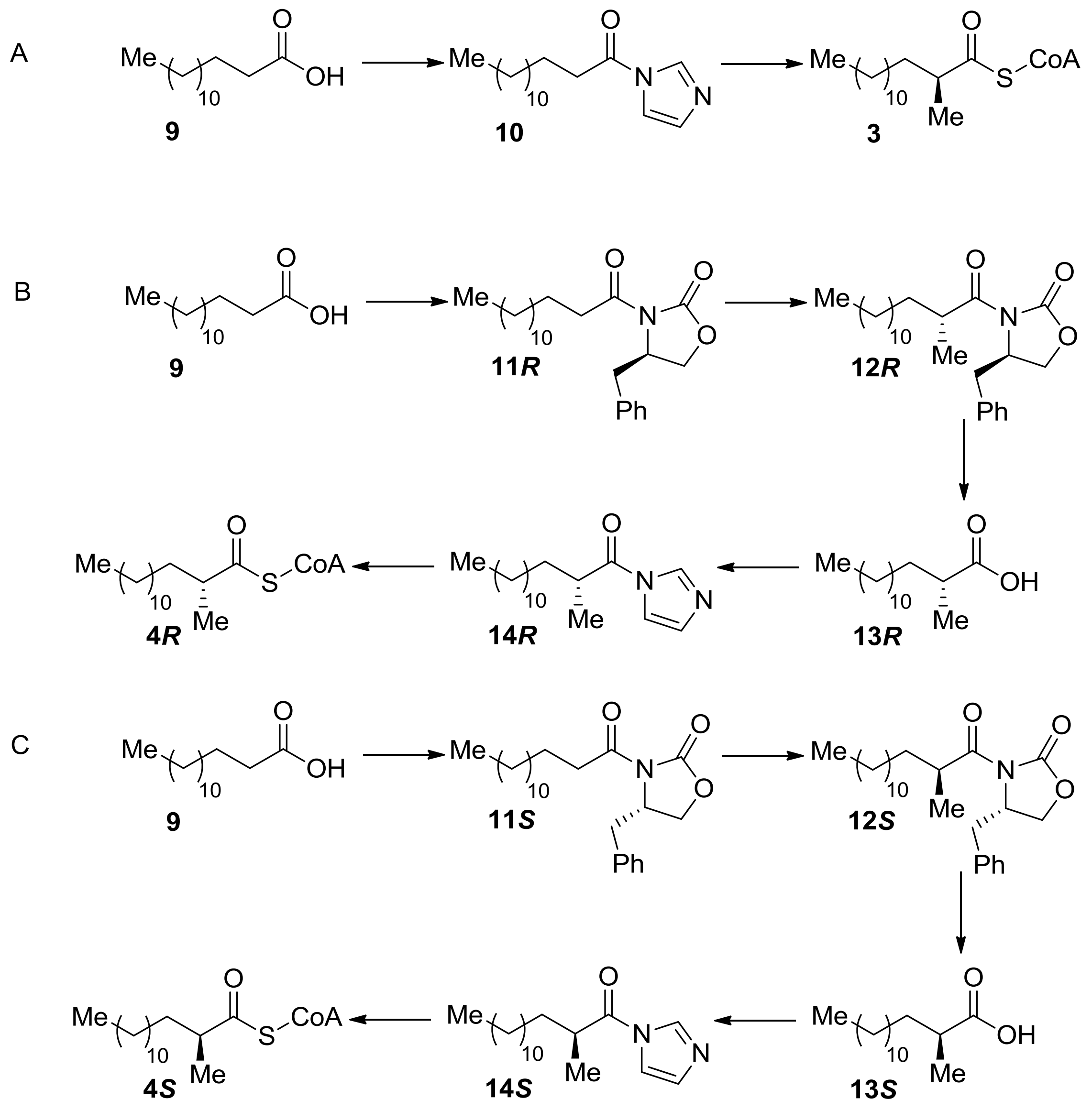

Scheme S1: Synthesis of substrates: A) Myristoyl-CoA **3**; B) *R*-2-methylmyristoyl-CoA **4*R***; C) *S*-2-methylmyristoyl-CoA **4*S***;

General experimental

All chemicals were obtained from the Sigma-Aldrich Chemical Co. or Fisher Scientific Ltd and were used without further purification, unless otherwise noted. Coenzyme A tri-lithium salt was purchased from Calbiochem. Reagents were of analytical grade or equivalent (synthesis) or biochemical grade. Sources of biological reagents are reported in the experimental section of the main paper. NMR spectra were recorded on either a JEOL GX 270 (270.05 MHz ^{1}H; 67.8 MHz ^{13}C) or a JEOL EX 400 (399.65 MHz ^{1}H; 100.4 MHz ^{13}C; 376.05 MHz) spectrometer. Spectra were referenced to the residual solvent peak, or externally via the solvent lock signal. Coupling constants (J) are reported in Hz to the nearest 0.1 Hz. Mass spectra were obtained using a VG 7070 mass spectrometer. Optical rotations were recorded on an Optical Activity AA-10 Automatic polarimeter with a path-length of 1 decimetre (1 dm). Concentrations (c) are quoted in g/100 mL. Column chromatography was performed using silica gel 60 (0.040-0.063 mm, Merck). Experiments were conducted at ambient temperature, unless otherwise stated. Solutions in organic solvents were dried using anhydrous sodium sulfate and solvents were evaporated under reduced pressure.

*Synthesis of 1-(1H-imidazol-1-yl)-tetradecan-1-one (**10**)*

A solution of myristic acid **9** (106 mg, 0.46 mmol) in dichloromethane (10 mL) was treated with solid portions of carbonyl di-imidazole (142 mg, 0.87 mmol) and the resulting reaction mixture was stirred under argon for 1 hour. The reaction mixture was washed with water (4 x 10 mL) and then dried over anhydrous sodium sulfate. Evaporation of the volatile organics gave a colourless solid **10**, 126 mg (98.5 %). ^{1}H-NMR (400.04 MHz, $CDCl_3$): δ = 0.88 (t, J = 6.5 Hz, 3H), 1.22-1.45 (m, 20H), 1.79 (pentet, J = 7.5 Hz, 2H), 2.85 (t, J = 7.4 Hz, 2H), 7.10 (m, 1H), 7.47 (t, J = 1.4 Hz, 1H), 8.16 (s, 1H).

*Synthesis of myristoyl-CoA (**3**)*

A solution of **10** (15 mg, 0.054 mmol) and coenzyme A, tri-lithium salt (14 mg, 0.018 mmol) were reacted in THF (1 mL) and aq. $NaHCO_3$ solution (1 mL, 0.1 M). The reaction was stirred under nitrogen for 16 hours. The reaction was acidified to pH 4.5 with HCl (1M) and then washed repeatedly with ethyl acetate (6 x 5 mL). Freeze-drying of the aqueous layer afforded **3** as a colourless solid (18 mg). ESI-MS m/z calcd. for $[M-H]^-$ $C_{35}H_{61}N_7O_{17}P_3S$: 976.3063; found 976.3016.

*Synthesis of S-4-Benzyl-3-tetradecanoyloxazolidin-2-one (**11S**)*

Oxalyl chloride (2.10 g, 3.2 ml, 16.7 mmol) was added slowly to a solution of myristic acid **9** (2.80 g, 12.3 mmol) in chloroform (20 mL) at 0 ºC. The reaction was allowed to warm to room temperature over 1 hour. Evaporation of the volatiles *in vacuo* afforded the acid chloride as a yellow oil (~3 mL). ^{n}BuLi (4.5 mL, 1.6 M, 7.2 mmol) was added dropwise to a solution of *S*-4-benzyloxazolidinone (1.20 g, 6.7 mmol) in dry THF (20 mL) at -78 ºC, followed by the acid chloride (2 mL). Addition of the acid chloride gave a colourless precipitate, which dissolved as the reaction was warmed to 0 ºC over 1 hour. The reaction was stirred at this temperature for a further hour and then quenched by the addition of a saturated ammonium chloride solution (10 mL). The reaction mixture was extracted with dichloromethane (3 x 25 mL). The combined organics were washed with aqueous K_2CO_3 (20 mL, 1M) and brine (20 mL). Drying over anhydrous sodium sulfate and removal of the volatiles *in vacuo* gave the crude product as a yellow oil (3.40 g). Purification by column chromatography (petroleum ether/ethyl acetate, 9:1) afforded a colourless oil that solidified on standing to a colourless solid, 1.79 g (69.0 %). ^{1}H-NMR (400.04 MHz, $CDCl_3$): δ = 0.88 (t, J = 6.6 Hz, 3H), 1.20-1.44 (m, 20H), 1.69 (quintet, J = 7.2 Hz, 2H), 2.76 (dd, J = 9.6, 13.4 Hz, 1H), 2.93 (m, 2H), 3.30 (dd, J = 3.3, 13.4 Hz, 1H), 4.17 (m, 2H), 4.67 (m, 1H), 7.20 (m, 2H), 7.26-7.36 (m, 3H).

*Synthesis of R-4-Benzyl-3-tetradecanoyloxazolidin-2-one (**11R**)*

In a parallel synthesis **11*R*** was obtained from myristic acid **9** (2.80 g, 12.3 mmol) and *R*-4-benzyloxazolidinone (1.20 g, 6.7 mmol) as a colourless oil which solidified on standing to a colourless solid, 2.50 g (96 %). NMR spectra were identical to **11*S***.

*Synthesis of 3-(S-2-Methyltetradecanoyl)-4-S-4-benzyloxazolidinone (**12S**)*

A solution of **11*S*** (1.70 g, 4.40 mmol) in dry THF (5 mL) was added dropwise to a cooled (-78 ºC) solution of lithium bis(trimethylsilyl)amide (8.8 mL, 1.0 M in THF, 8.8 mmol), under an argon atmosphere. The reaction mixture was stirred for 1 hour at this temperature before methyl iodide (1.4 mL, 3.12g, 22 mmol) in THF (0.5 mL) at -78 ºC was added. The reaction was stirred for a further 3 hours at -78 ºC and then allowed to warm to 0 ºC. The reaction was quenched with saturated ammonium chloride (15 mL) and then extracted with dichloromethane (3 x 20 mL). The combined organics were washed with aqueous sodium sulfite (1M) and then dried over anhydrous sodium sulfate. Evaporation of the volatile organics afforded an orange oil. Purification by flash chromatography (petroleum ether/ethyl acetate, 20:1) gave **12*S*** as a colourless oil, 560 mg (31.1 %). ^{1}H-NMR (400.04 MHz, $CDCl_3$): δ = 0.88 (t, J = 6.6 Hz, 3H), 1.22 (d, J = 6.8 Hz, 3H), 1.22-1.35 (m, 20H), 1.36-1.47 (m, 1H), 1.73 (m, 1H), 2.76 (dd, J = 9.6, 13.3 Hz, 1H), 3.27 (dd, J = 3.2, 13.4 Hz, 1H), 3.70 (sextet, J = 6.6 Hz, 1H), 4.11-4.22 (m, 2H), 4.67 (m, 1H), 7.21 (m, 2H), 7.24-7.36 (m, 3H).

*Synthesis of 3-(R-2-Methyltetradecanoyl)-4-R-4-benzyloxazolidinone (**12R**)*

Treatment of **11*R*** (2.5g, 6.5 mmol) with lithium bis(trimethylsilyl)amide (8.8 mL, 1.0M in THF, 8.8 mmol) and methyl iodide (4.56g, 2.0 mL, 32.5 mmol), as for the synthesis of **12*S***, afforded **12*R*** as a colourless oil, 690 mg (26.4 %). NMR spectra were identical to **12*S***.

*Synthesis of S-2-Methyltetradecanoic acid (**13S**)*

A solution of **12*S*** (550 mg, 1.4 mmol) in THF (25 mL) and water (8 mL) at 0 ºC was treated with hydrogen peroxide (1.2 mL, 30 %) and lithium hydroxide (70 mg, 2.8 mmol). The reaction was maintained at this temperature for 3 hours and then quenched with aqueous sodium sulfite (11 mL, 1.5 M). The reaction mixture was acidified to pH 1 with HCl (1M) and then extracted with dichloromethane (3 x 25 mL). The combined extracts were dried over sodium sulfate and then evaporated *in vacuo* to give a colourless oil. Purification by flash chromatography (petroleum ether/ethyl acetate, 3:2) gave **13*S*** as a colourless oil, 270 mg (80 %). ^{1}H-NMR (400.04 MHz, $CDCl_3$): δ = 0.88 (t, J = 6.6 Hz, 3H), 1.18 (d, J = 7.0 Hz, 3H), 1.22-1.37 (m, 20H), 1.37-1.48 (m, 1H), 1.63-1.73 (m, 1H), 2.46 (sextet, J = 6.9 Hz, 1H). ^{13}C-NMR (125. MHz, $CDCl_3$): δ = 14.10, 16.80, 22.69, 27.15, 29.48, 29.52, 29.61, 29.65, 29.68, 31.93, 39.42, 183.63. $[\alpha]_D^{20}$ = +23.8 ° (*c* 0.034, methanol).

*Synthesis of R-2-Methyltetradecanoic acid (**13R**)*

Treatment of **12*R*** (690 mg, 1.72 mmol) with lithium hydroxide (82 mg, 3.44 mmol) and hydrogen peroxide (1.5 mL, 30 % in H_2O) as for the synthesis of **13*S***, afforded **13*R*** as a colourless oil which solidified on standing to a colourless solid, 280 mg (67.3 %). NMR spectra were identical to **13*S***. $[\alpha]_D^{20}$ = -23.9 º (*c* 0.014, methanol)

*Synthesis of S-1-(1H-imidazol-1-yl)-2-methyltetradecan-1-one (**14S**)*

A solution of **13*S*** (100 mg, 0.41 mmol) in dichloromethane (10 mL) was treated with carbonyl di-imidazole (133 mg, 0.82 mmol) in dichloromethane as described for the synthesis of **10**. Evaporation of the volatile organics gave a colourless oil which solidified on standing to give a colourless solid **14*S***, 130 mg (92 %).^{1}H-NMR (400.04 MHz, $CDCl_3$): δ = 0.88 (t, J = 6.5 Hz, 3H), 1.22-1.33 (m, 22H), 1.50-1.61 (m, 1H), 1.80-1.89 (m, 1H), 3.05 (sextet, J = 6.8 Hz, 1H), 7.11 (t, J = 0.8 Hz, 1H), 7.49 (d, J = 1.4 Hz, 1H), 8.17 (s, 1H).

*Synthesis of R-1-(1H-imidazol-1-yl)-2-methyltetradecan-1-one (**14R**)*

As for the synthesis of **14*S***, **14*R*** was prepared by treatment of **13*R*** (100 mg, 0.41 mmol) with carbonyl di-imidazole (133 mg, 0.82 mmol) in dichloromethane. **14*R*** was obtained as a colourless oil that solidified on standing to give a colourless solid, 115 mg (96.1 %). NMR spectra were identical to **14*S***.

*Synthesis of S-2-Methylmyristoyl-CoA (**4S**)*

A solution of **14*S*** (12 mg, 0.041 mmol) in THF (1 mL) and coenzyme A, tri-lithium salt (11 mg, 0.014 mmol) in THF (1 mL) and aq. $NaHCO_3$ solution were reacted as described for the synthesis of **3**. Freeze-drying of the aqueous layer afforded **4*S*** as a colourless solid (14 mg). ESI-MS m/z calcd. for $[M-H]^-$ $C_{36}H_{63}N_7O_{17}P_3S$: 990.3219; found 990.3177.

*Synthesis of R-2-Methylmyristoyl-CoA (**4R**)*

In similar fashion to the preparation of **4*S***, **4*R*** was obtained from the reaction of **14*R*** (15 mg, 0.051 mmol) and coenzyme A, tri-lithium salt (14 mg, 0.018 mmol) in THF (1 mL) and aq. $NaHCO_3$ solution (1 mL, 0.1 M). Freeze-drying gave **4*R*** as a colourless solid (18 mg). ESI-MS m/z calcd. for $[M-H]^-$ $C_{36}H_{63}N_7O_{17}P_3S$: 990.3219; found 990.3176.

Myristoyl-CoA 3, ACOT-1

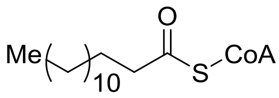

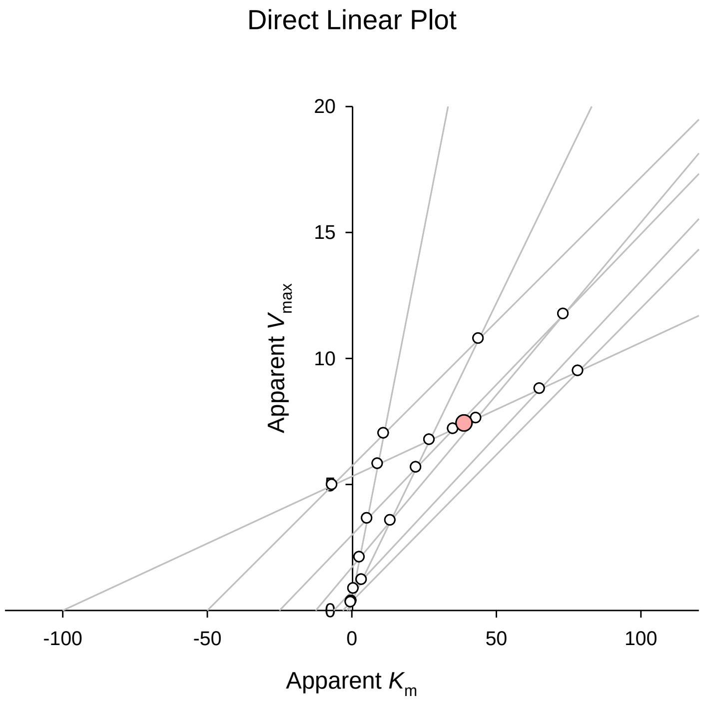

Michaelis-Menten

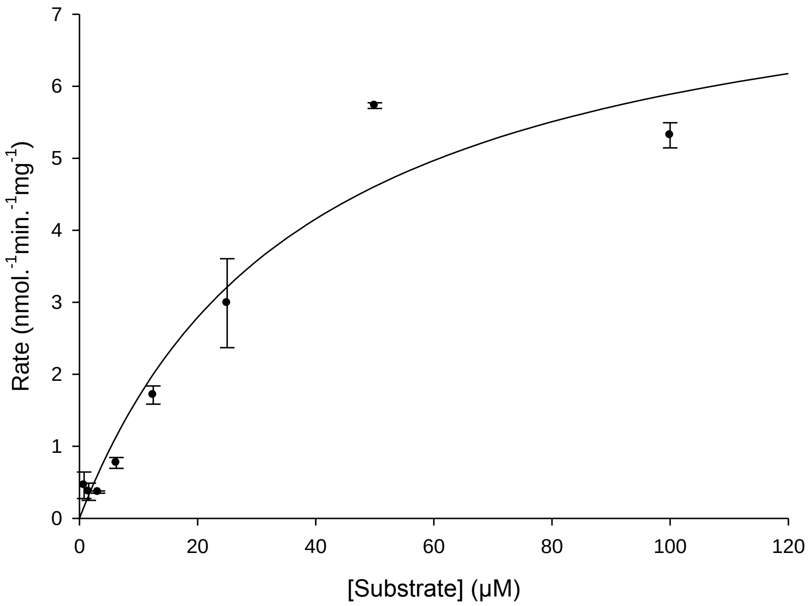

Parameters

	Value	±Std. Error	95% Conf. Interval		
V_{max}	8.1547	0.9661	6.1511	to	10.1583
K_m	38.4668	10.2782	17.1507	to	59.7828

Goodness of Fit

Degrees of Freedom	22
AICc	-16.555
R^2	0.917
Sum of Squares	8.920
Sy.x	0.637
Runs Test p Value	0.456

Data

Number of x values	8
Number of replicates	3
Total number of values	24
Number of missing values	0

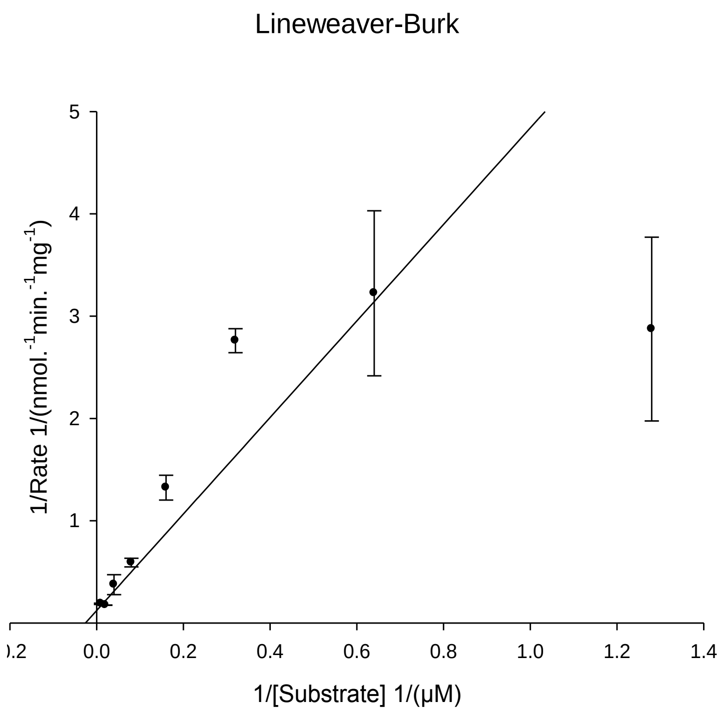

Lineweaver-Burk
5
4
3
2
1
1/Rate 1/(nmol.-1min.-1mg-1)
).2
0.0
0.2
0.4
0.6
0.8
1.0
1.2
1.4
1/[Substrate] 1/(µM)

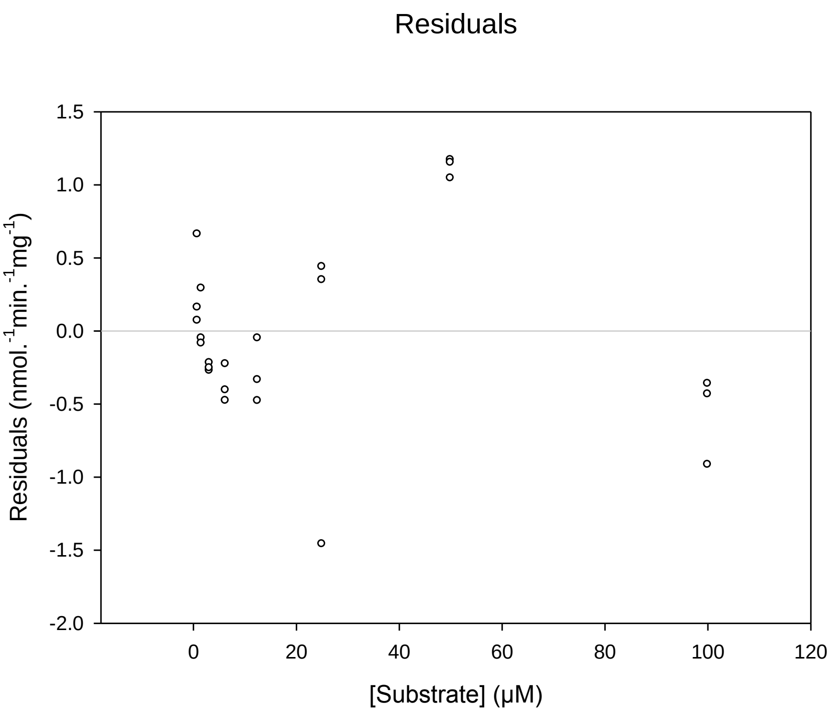

Residuals
1.5
1.0
0.5
0.0
-0.5
-1.0
-1.5
-2.0
Residuals (nmol.-1min.-1mg-1)
0
20
40
60
80
100
120
[Substrate] (µM)

R-2-Methylmyristoyl-CoA 4R, ACOT-1

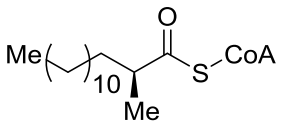

Direct Linear Plot

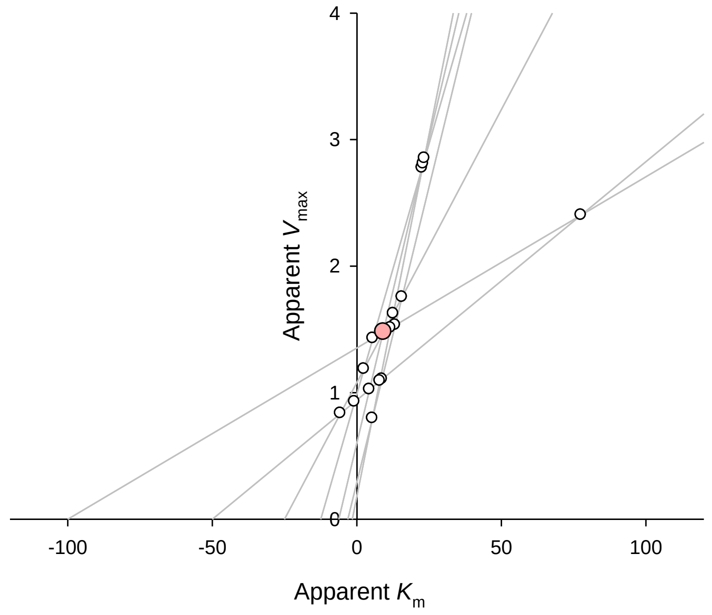

Michaelis-Menten

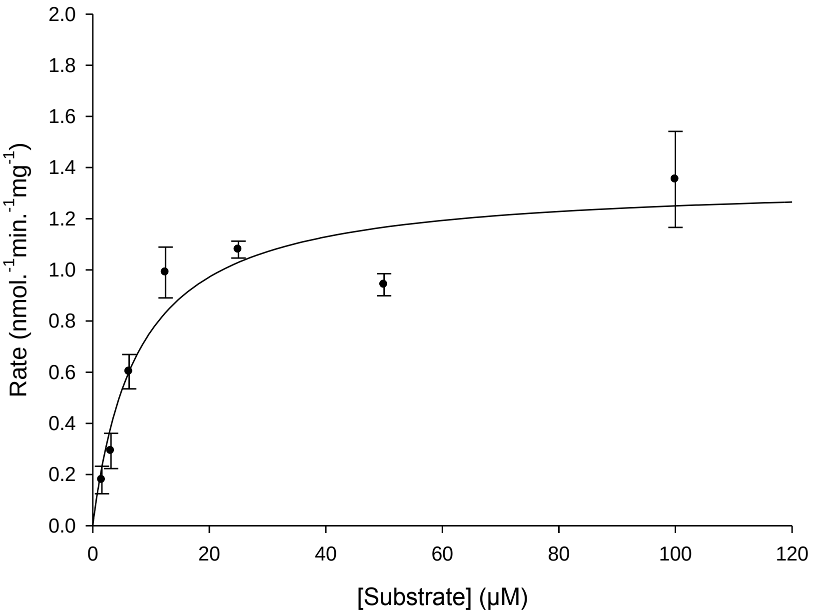

Parameters

	Value	±Std. Error	95% Conf. Interval		
V_{max}	1.3465	0.1023	1.1324	to	1.5606
K_m	7.7008	2.0800	3.3472	to	12.0544

Goodness of Fit

Degrees of Freedom	19
AICc	-65.237
R^2	0.822
Sum of Squares	0.660
Sy.x	0.186
Runs Test p Value	0.254

Data

Number of x values	7
Number of replicates	3
Total number of values	21
Number of missing values	0

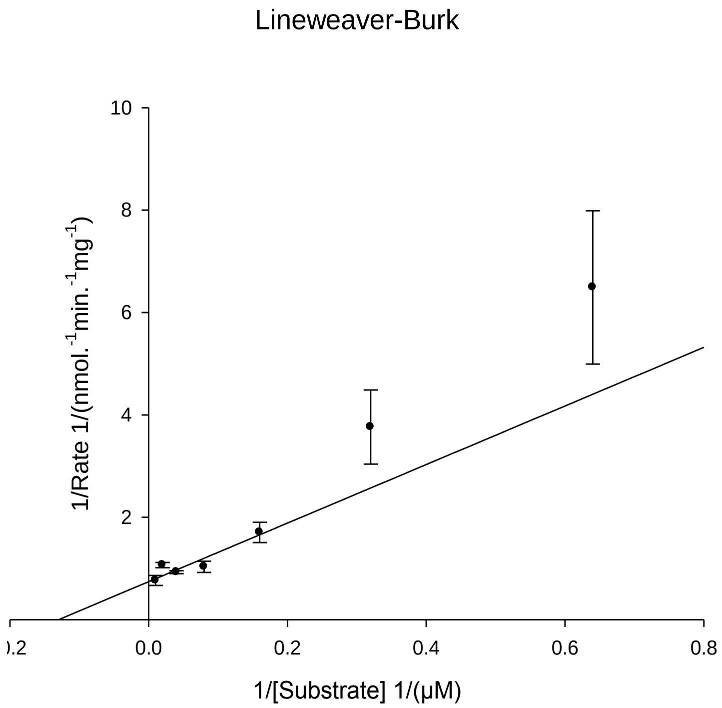
Lineweaver-Burk
10
8
6
4
2
1/Rate 1/(nmol.-1min.-1mg-1)
0.2
0.0
0.2
0.4
0.6
0.8
1/[Substrate] 1/(µM)

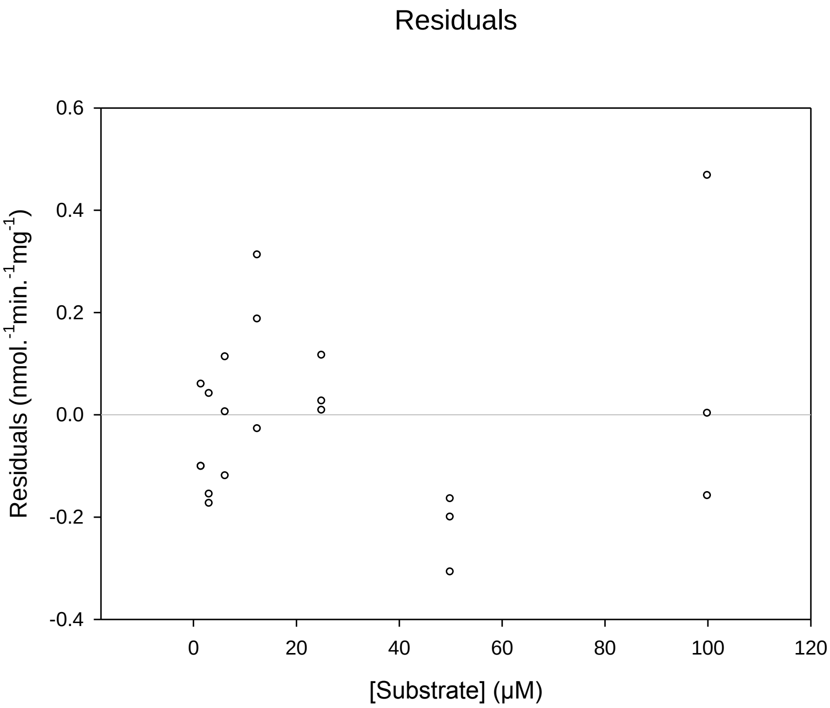
Residuals
0.6
0.4
0.2
0.0
-0.2
-0.4
Residuals (nmol.-1min.-1mg-1)
0
20
40
60
80
100
120
[Substrate] (µM)

S-2-Methylmyristoyl-CoA 4*S*, ACOT-1

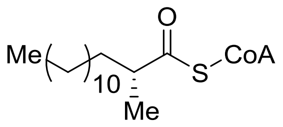

Direct Linear Plot

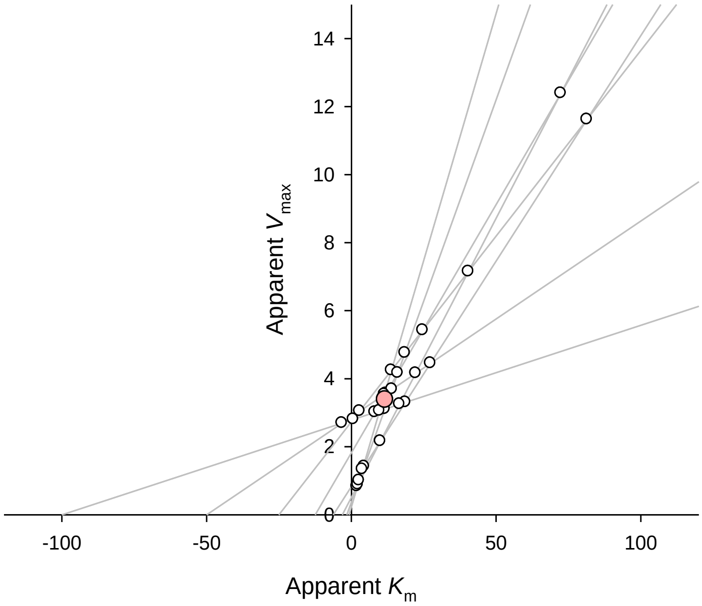

Michaelis-Menten

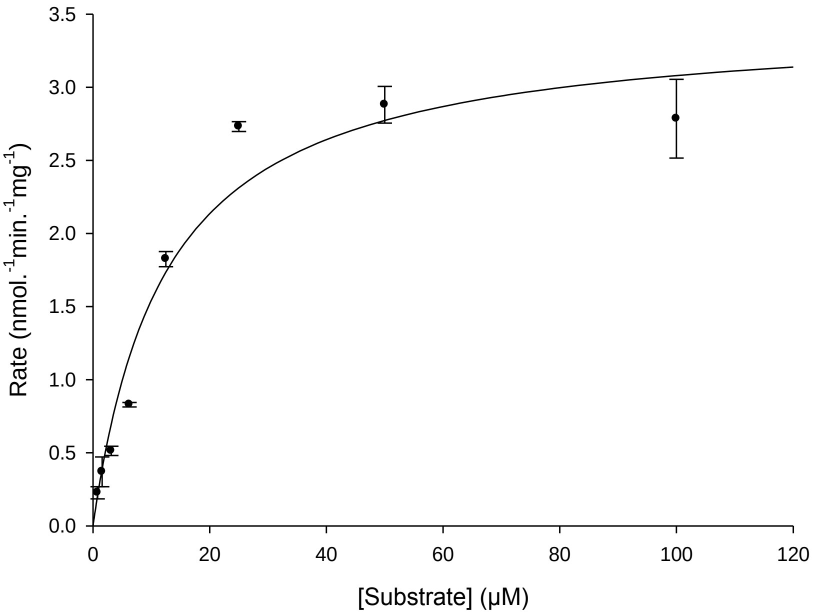

Parameters

	Value	±Std. Error	95% Conf. Interval		
V_{max}	3.4628	0.2008	3.0464	to	3.8792
K_m	12.4377	2.2548	7.7615	to	17.1139

Goodness of Fit

Degrees of Freedom	22
AICc	-53.600
R^2	0.935
Sum of Squares	1.905
Sy.x	0.294
Runs Test p Value	0.050

Data

Number of x values	8
Number of replicates	3
Total number of values	24
Number of missing values	0

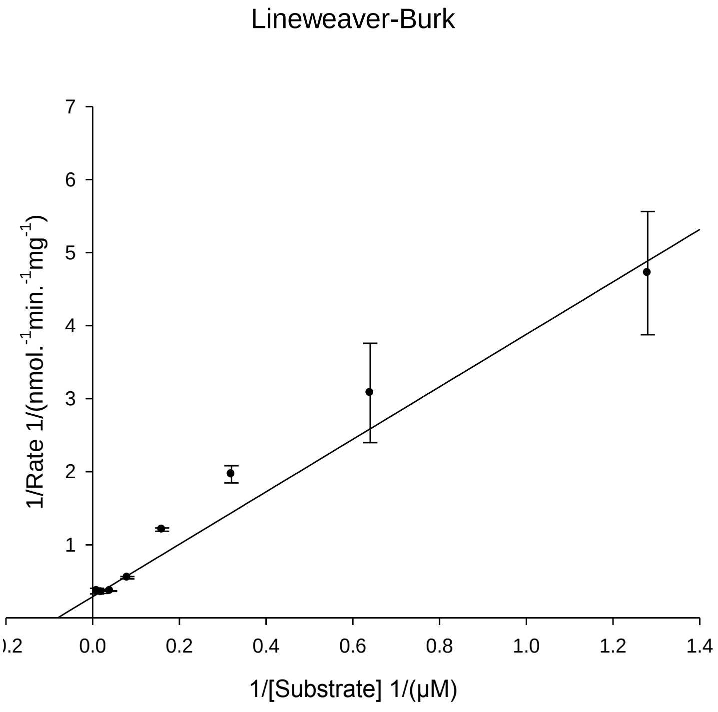

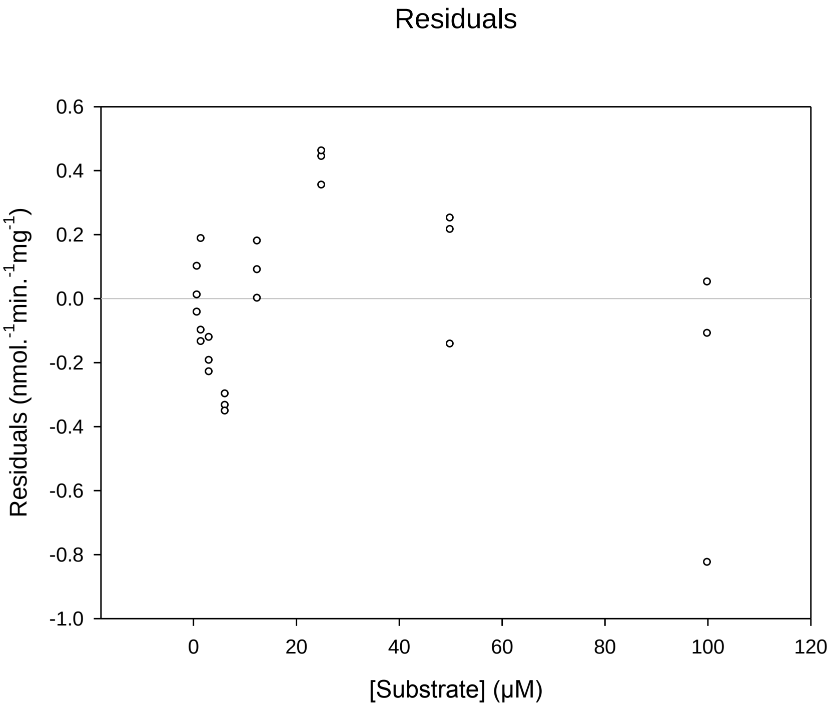

±-Fenoprofenoyl-CoA 5, ACOT-1

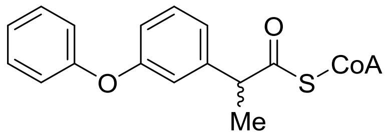
O
O
S
CoA
Me

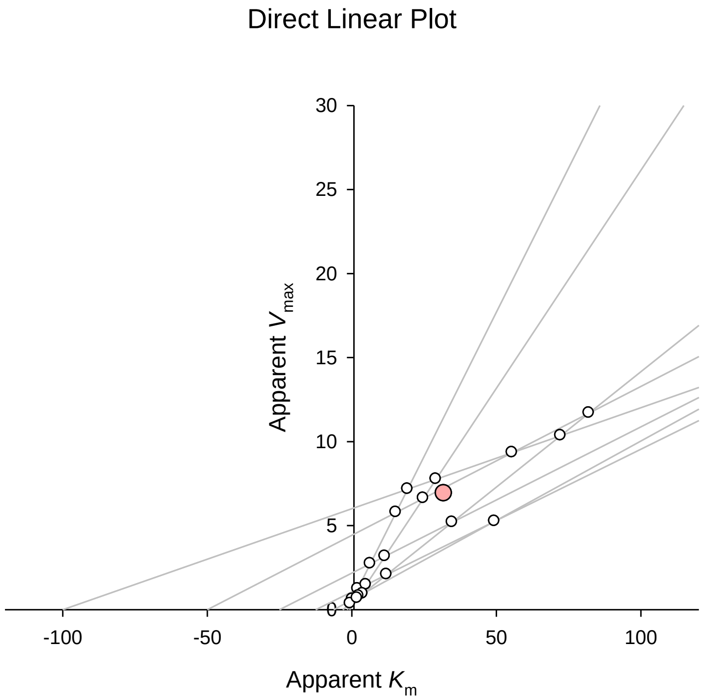
Direct Linear Plot
30
25
20
15
10
5
0
Apparent V_{max}
-100
-50
0
50
100
Apparent K_m

Michaelis-Menten

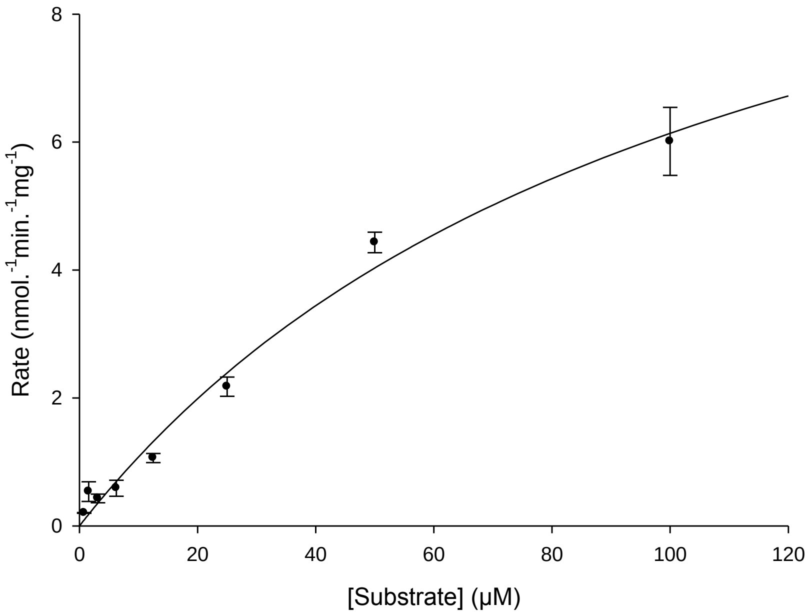

Parameters

	Value	±Std. Error	95% Conf. Interval		
V_{max}	12.8319	2.0165	8.6498	to	17.0140
K_m	109.0979	27.7494	51.5481	to	166.6477

Goodness of Fit

Degrees of Freedom	22
AICc	-38.315
R^2	0.964
Sum of Squares	3.602
Sy.x	0.405
Runs Test p Value	0.237

Data

Number of x values	8
Number of replicates	3
Total number of values	24
Number of missing values	0

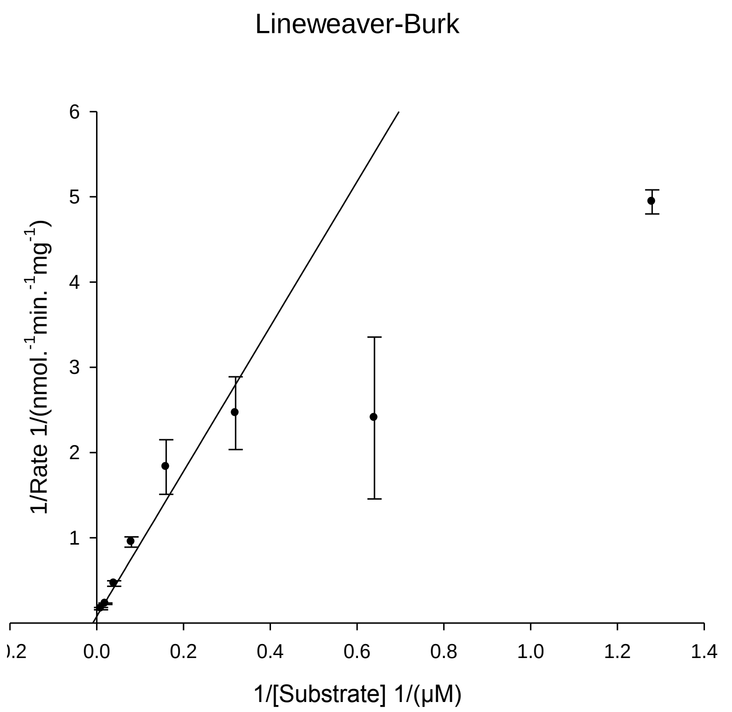

Lineweaver-Burk
1/Rate 1/(nmol.-1min.-1mg-1)
6
5
4
3
2
1
-0.2
0.0
0.2
0.4
0.6
0.8
1.0
1.2
1.4
1/[Substrate] 1/(µM)

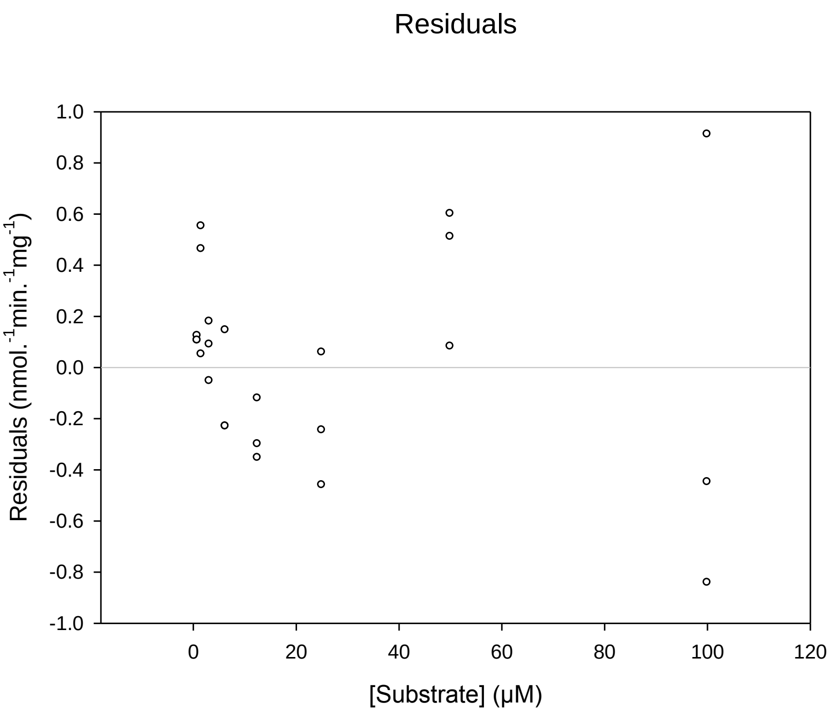

Residuals
Residuals (nmol.-1min.-1mg-1)
1.0
0.8
0.6
0.4
0.2
0.0
-0.2
-0.4
-0.6
-0.8
-1.0
0
20
40
60
80
100
120
[Substrate] (µM)

±-Flurbiprofenoyl-CoA 6, ACOT-1

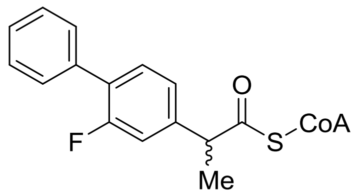

Direct Linear Plot

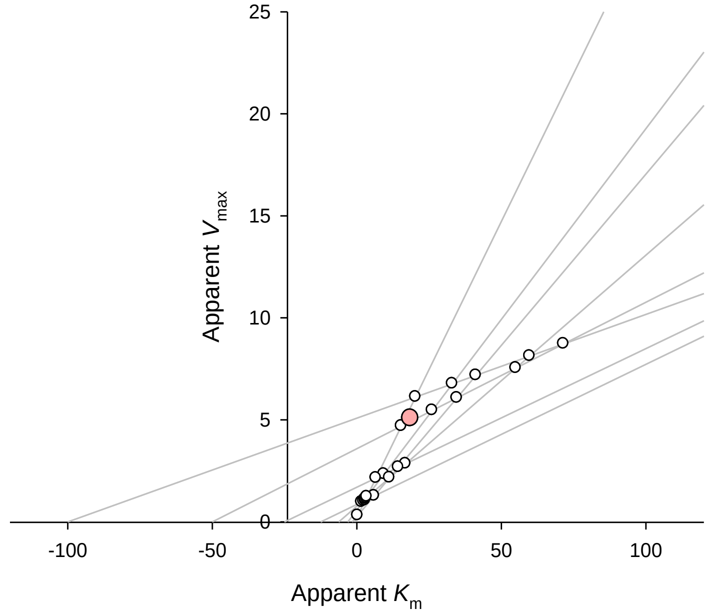

Parameters

	Value	±Std. Error	95% Conf. Interval		
V_{max}	11.2139	1.6125	7.8697	to	14.5582
K_m	117.8644	26.8142	62.2541	to	173.4747

Goodness of Fit

Degrees of Freedom	22
AICc	-54.182
R^2	0.972
Sum of Squares	1.860
Sy.x	0.291
Runs Test p Value	0.216

Data

Number of x values	8
Number of replicates	3
Total number of values	24
Number of missing values	0

Michaelis-Menten

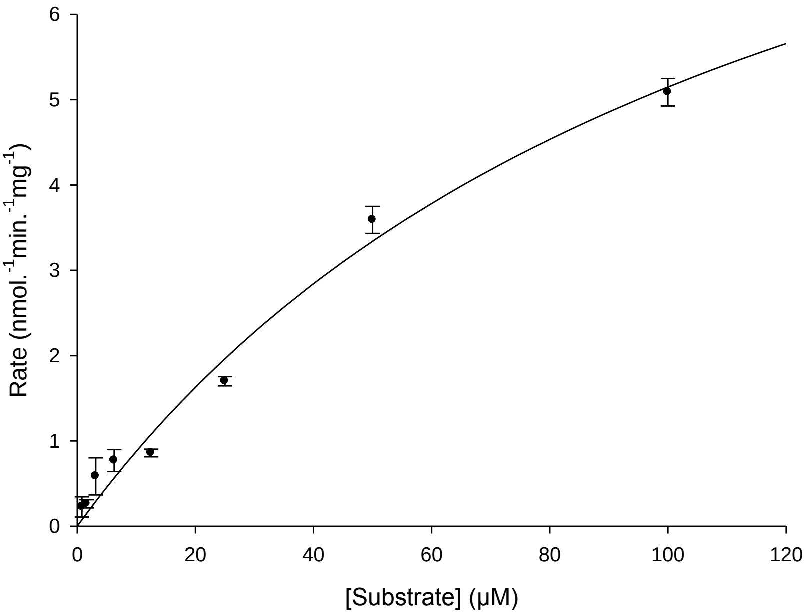

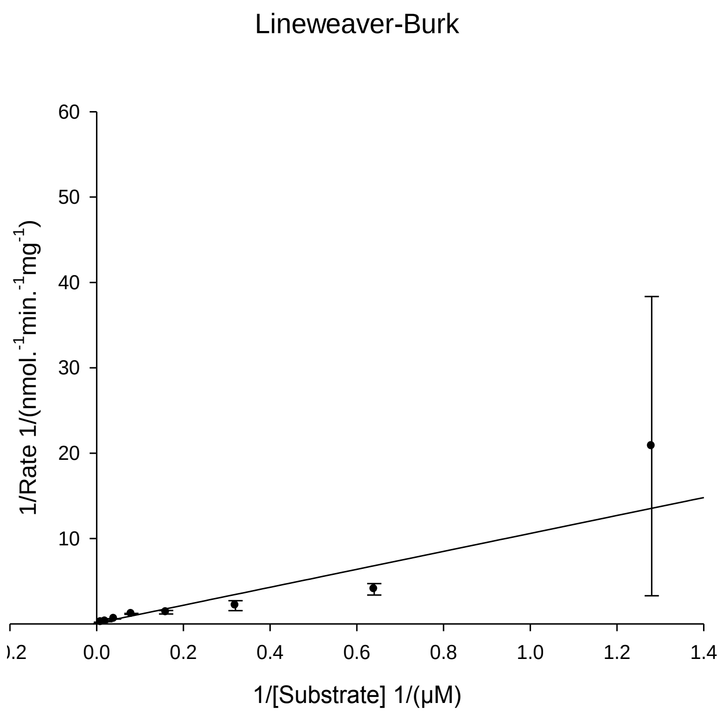
Lineweaver-Burk
1/Rate 1/(nmol.-1min.-1mg-1)
60
50
40
30
20
10
).2
0.0
0.2
0.4
0.6
0.8
1.0
1.2
1.4
1/[Substrate] 1/(µM)

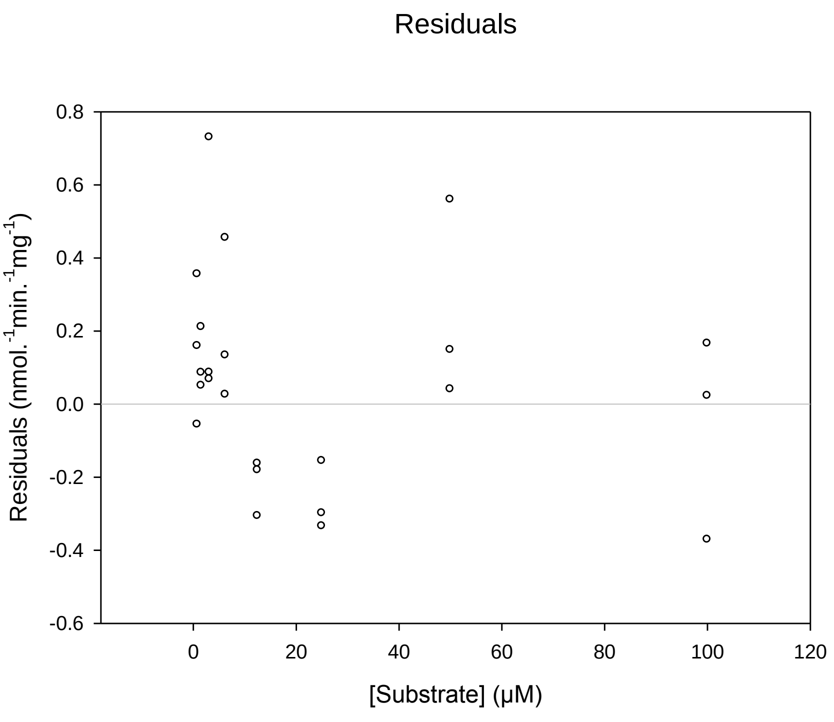
Residuals
Residuals (nmol.-1min.-1mg-1)
0.8
0.6
0.4
0.2
0.0
-0.2
-0.4
-0.6
0
20
40
60
80
100
120
[Substrate] (µM)

±-Ibuprofenoyl-CoA 2, ACOT-1

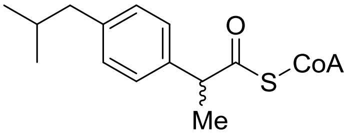

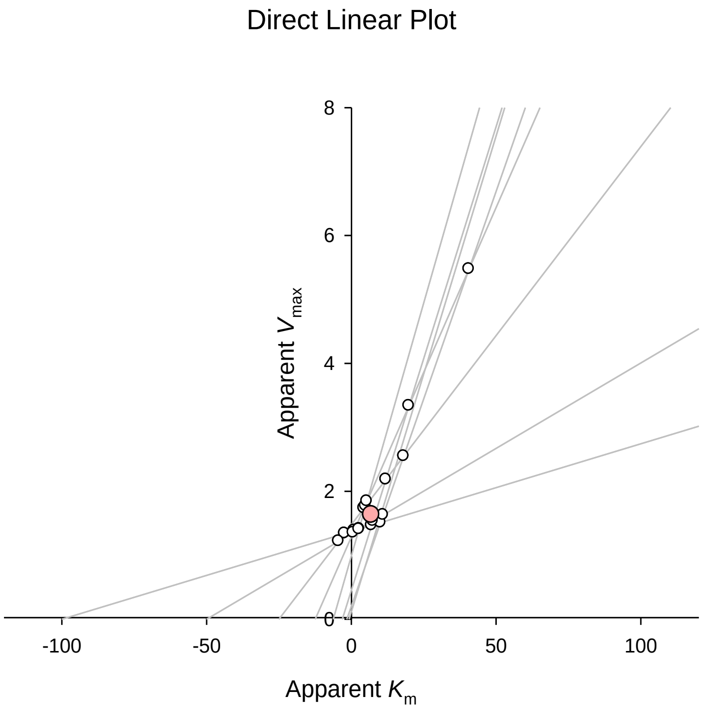

Enzyme Kinetics Nonlinear Fit Results

Notebook1
13/08/2011 20:04:09
Michaelis-Menten
Number of Replicates: 3

Parameters

	Value	±Std. Error	95% Conf. Interval		
V_{max}	1.5811	0.1008	1.3714	to	1.7908
K_m	5.0993	1.2597	2.4796	to	7.7190

Goodness of Fit

Degrees of Freedom	21
AICc	-65.326
R^2	0.849
Sum of Squares	0.980
Sy.x	0.216
Runs Test p Value	0.158

Data

Number of x values	8
Number of replicates	3
Total number of values	23
Number of missing values	1

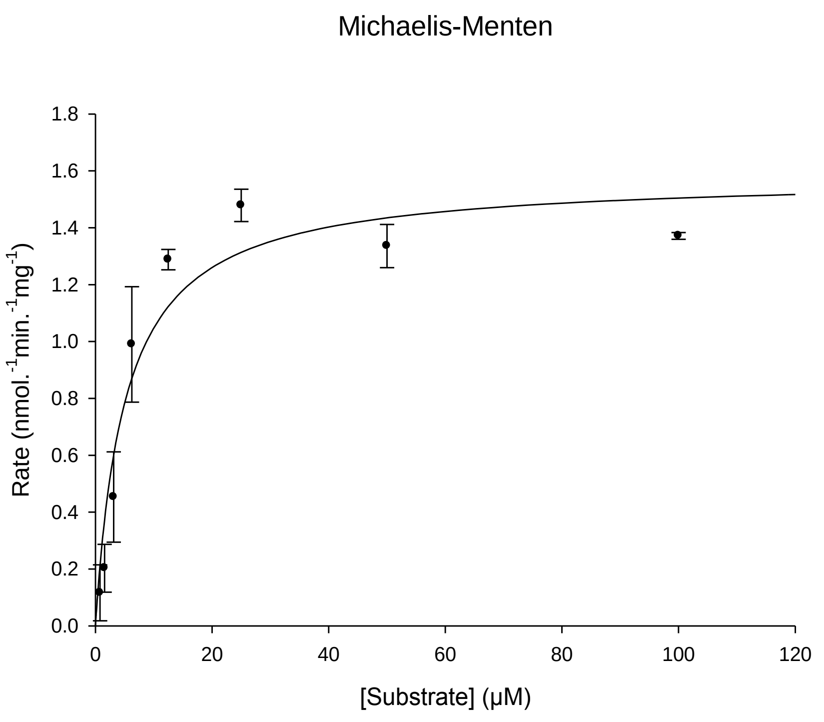

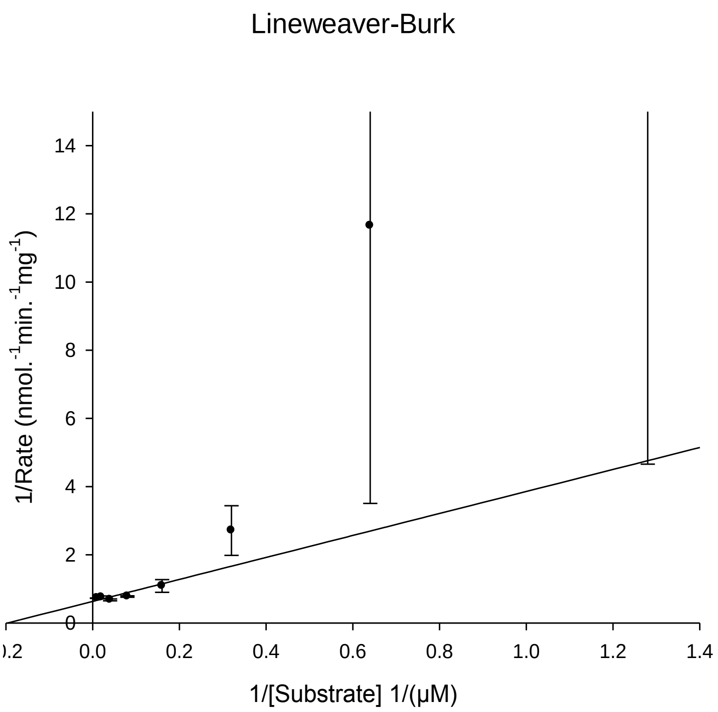
Lineweaver-Burk
1/Rate (nmol.$^{-1}$min.$^{-1}$mg^{-1})
14
12
10
8
6
4
2
0
-0.2
0.0
0.2
0.4
0.6
0.8
1.0
1.2
1.4
1/[Substrate] 1/(µM)

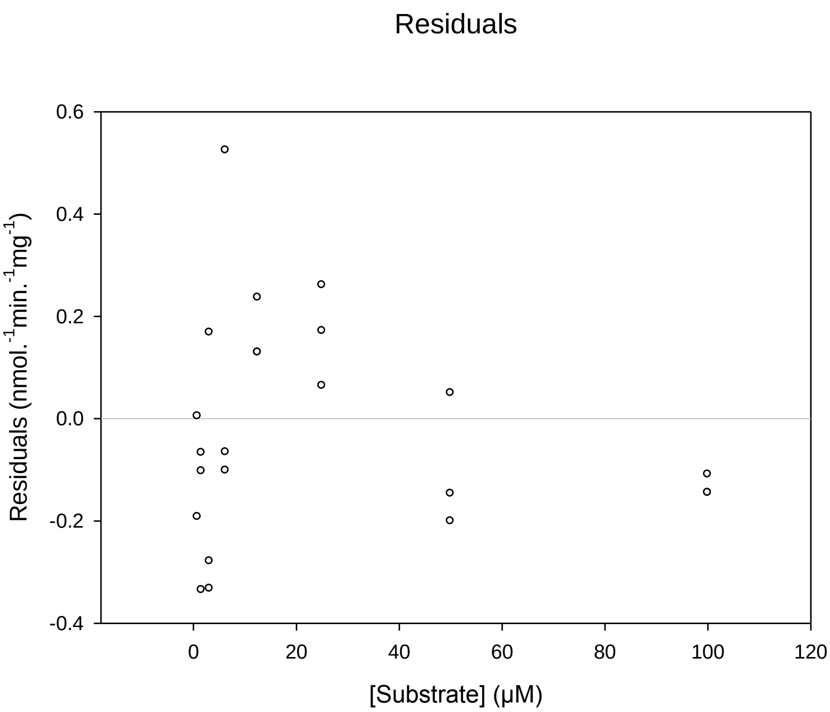
Residuals
Residuals (nmol.$^{-1}$min.$^{-1}$mg^{-1})
0.6
0.4
0.2
0.0
-0.2
-0.4
0
20
40
60
80
100
120
[Substrate] (µM)

S-Ketoprofenoyl-CoA 7, ACOT-1

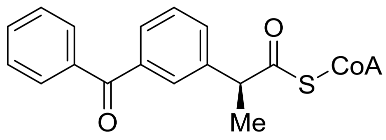

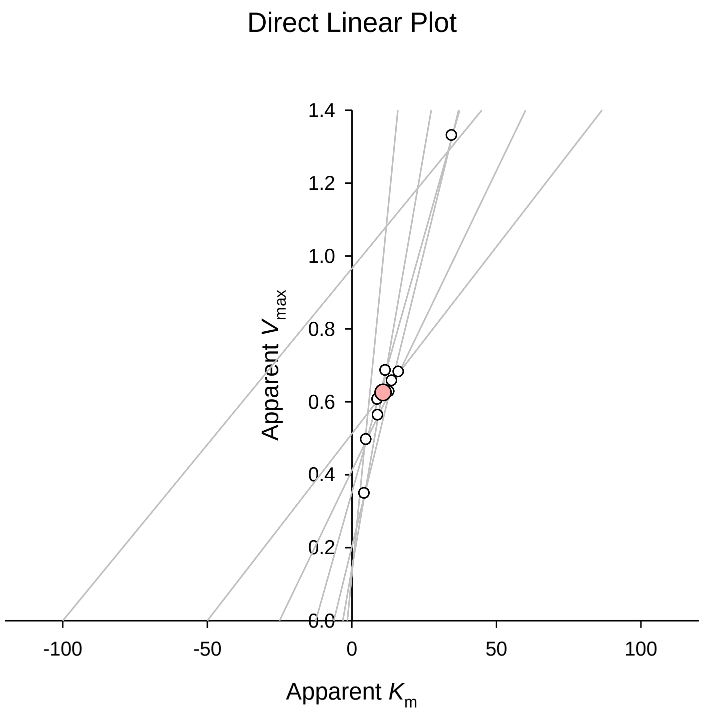

Parameters

	Value	±Std. Error	95% Conf. Interval		
V_{max}	1.2309	0.3441	0.5015	to	1.9604
K_m	44.7606	25.5387	-9.3801	to	98.9013

Goodness of Fit

Degrees of Freedom	16
AICc	-57.669
R^2	0.664
Sum of Squares	0.476
Sy.x	0.173
Runs Test p Value	0.213

Data

Number of x values	7
Number of replicates	3
Total number of values	18
Number of missing values	3

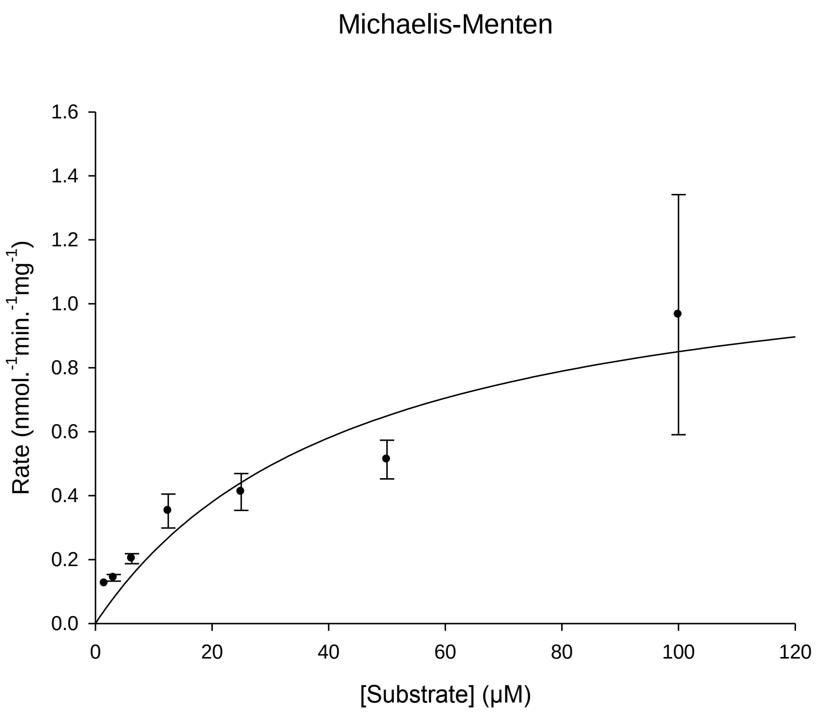

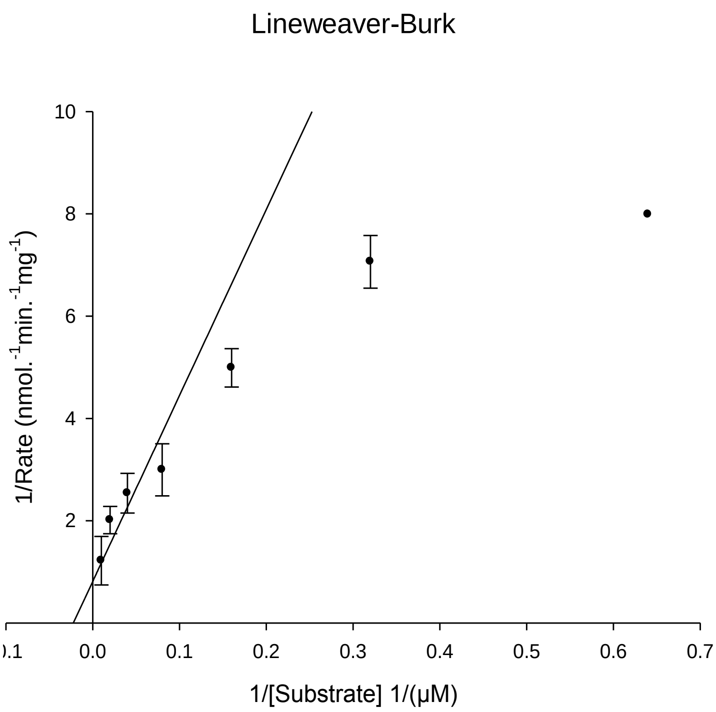
Lineweaver-Burk
1/Rate (nmol.-1min.-1mg-1)
1/[Substrate] 1/(µM)

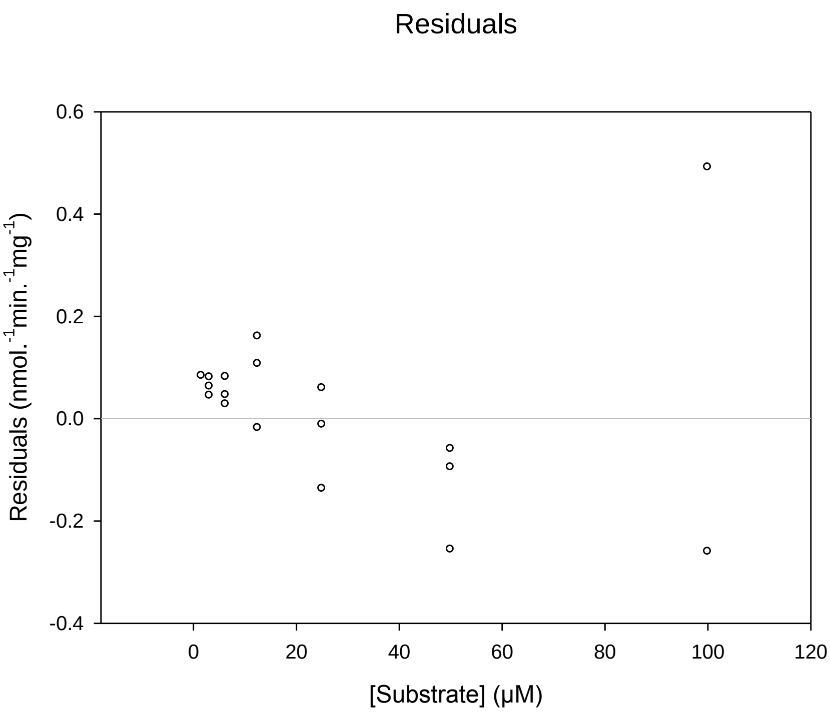
Residuals
Residuals (nmol.-1min.-1mg-1)
[Substrate] (µM)

S-Naproxenoyl-CoA 8, ACOT-1

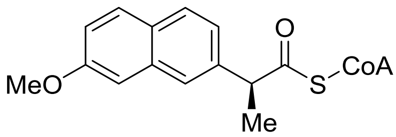

Direct Linear Plot

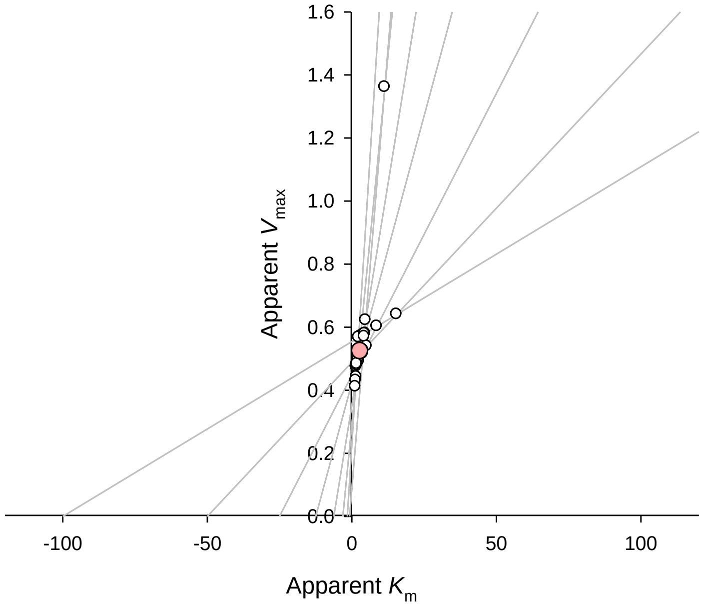

Parameters

	Value	±Std. Error	95% Conf. Interval		
V_{max}	0.5278	2.638e-2	0.4731	to	0.5825
K_m	2.7646	0.6042	1.5116	to	4.0177

Goodness of Fit

Degrees of Freedom	22
AICc	-123.839
R^2	0.823
Sum of Squares	0.102
Sy.x	6.812e-2
Runs Test p Value	0.076

Data

Number of x values	8
Number of replicates	3
Total number of values	24
Number of missing values	0

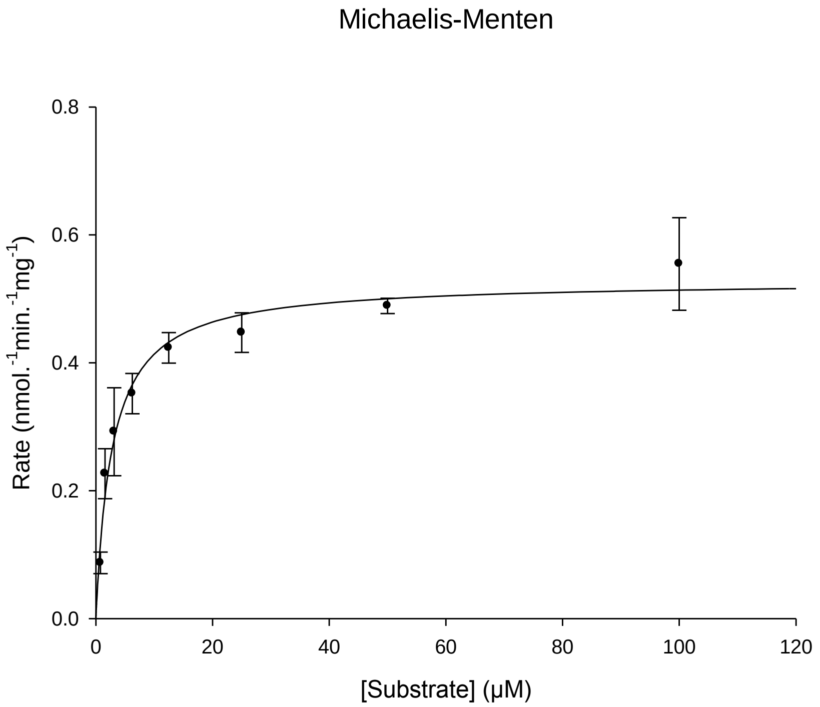

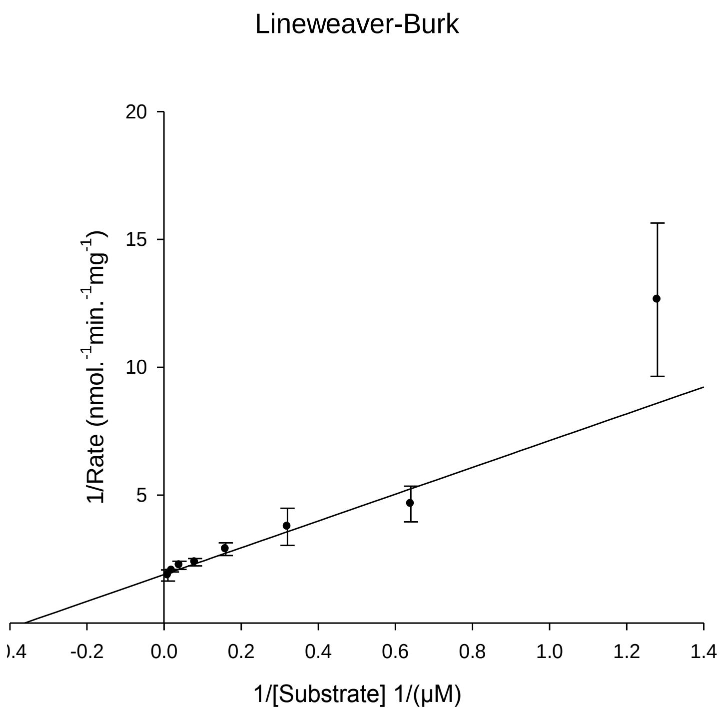
Lineweaver-Burk
1/Rate (nmol.-1min.-1mg-1)
20
15
10
5
0.4
-0.2
0.0
0.2
0.4
0.6
0.8
1.0
1.2
1.4
1/[Substrate] 1/(µM)

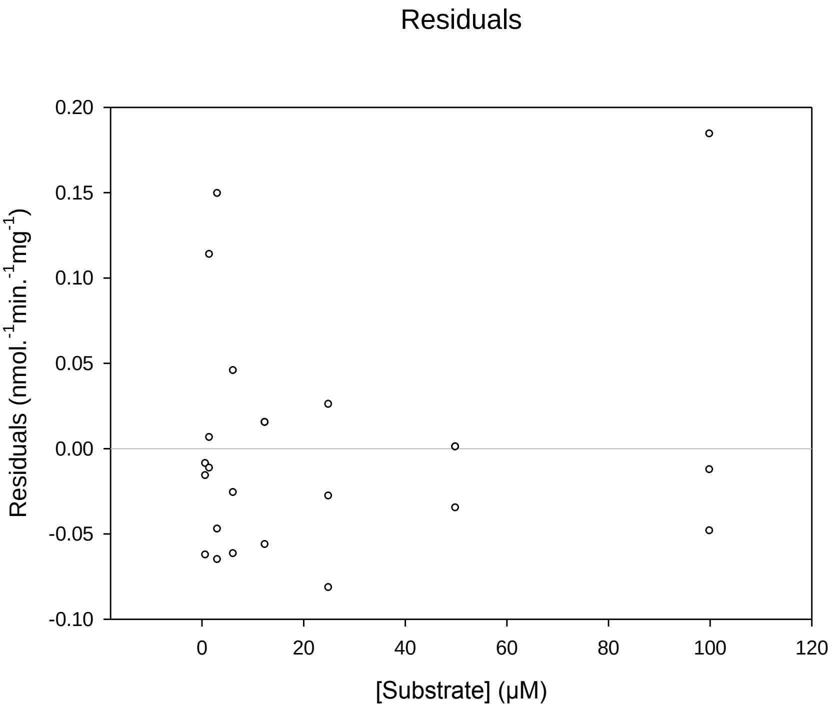
Residuals
Residuals (nmol.-1min.-1mg-1)
0.20
0.15
0.10
0.05
0.00
-0.05
-0.10
0
20
40
60
80
100
120
[Substrate] (µM)

Myristoyl-CoA 3, ACOT-2

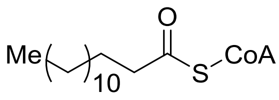

Direct Linear Plot

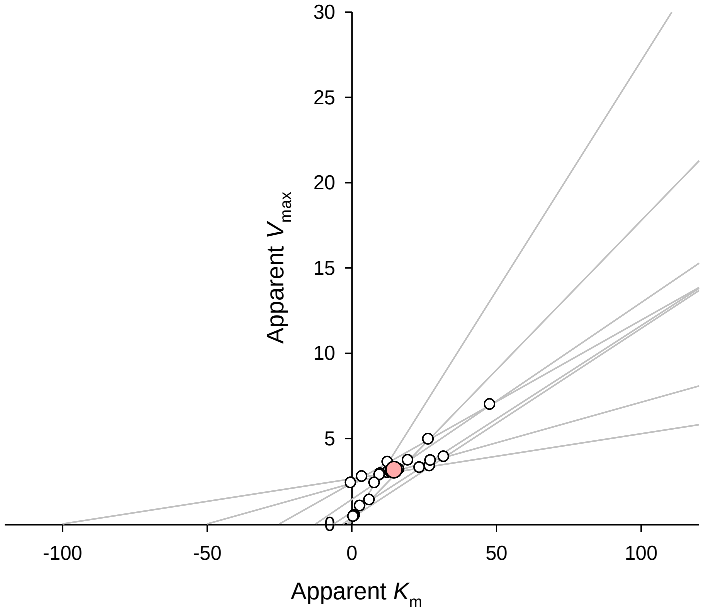

Michaelis-Menten

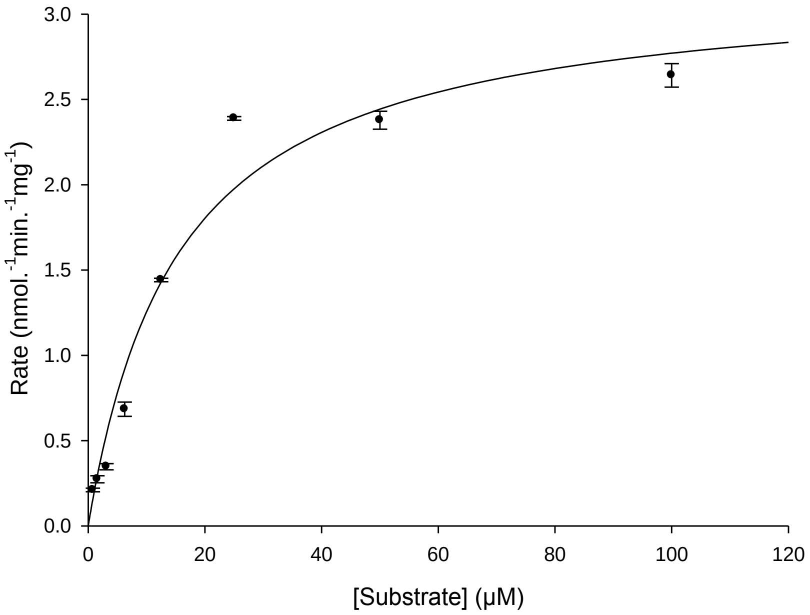

Parameters

	Value	±Std. Error	95% Conf. Interval		
V_{max}	3.2003	0.1581	2.8724	to	3.5282
K_m	15.4965	2.2602	10.8090	to	20.1840

Goodness of Fit

Degrees of Freedom	22
AICc	-70.983
R^2	0.960
Sum of Squares	0.924
Sy.x	0.205
Runs Test p Value	0.443

Data

Number of x values	8
Number of replicates	3
Total number of values	24
Number of missing values	0

Lineweaver-Burk

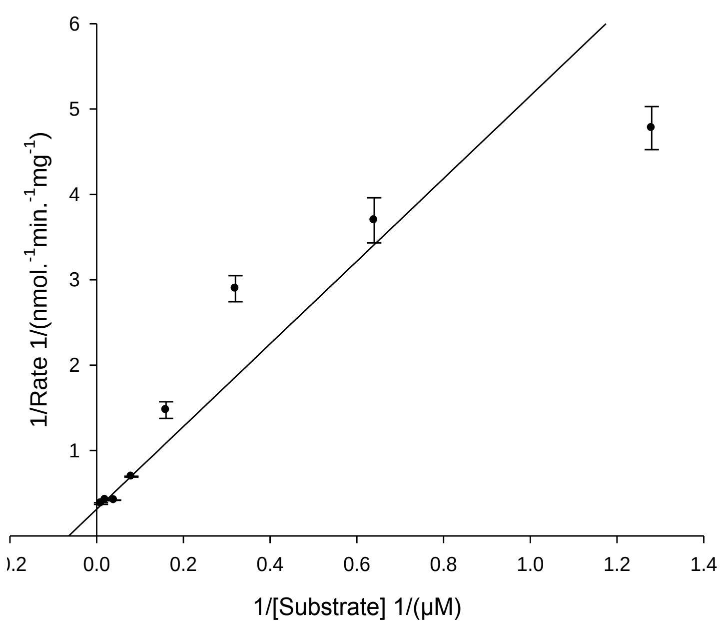

Residuals

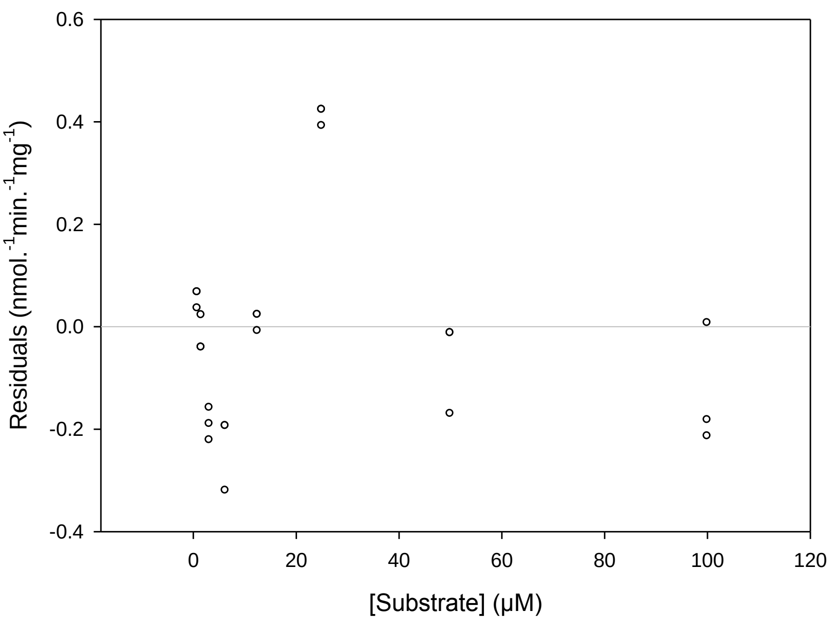

R-2-Methylmyristoyl-CoA 4*R*, ACOT-2

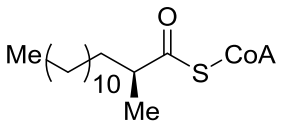

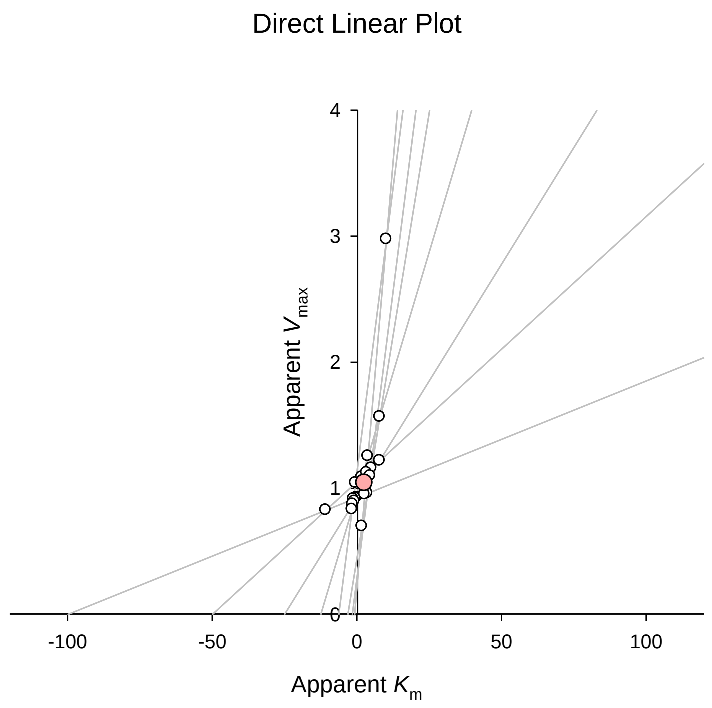

Michaelis-Menten

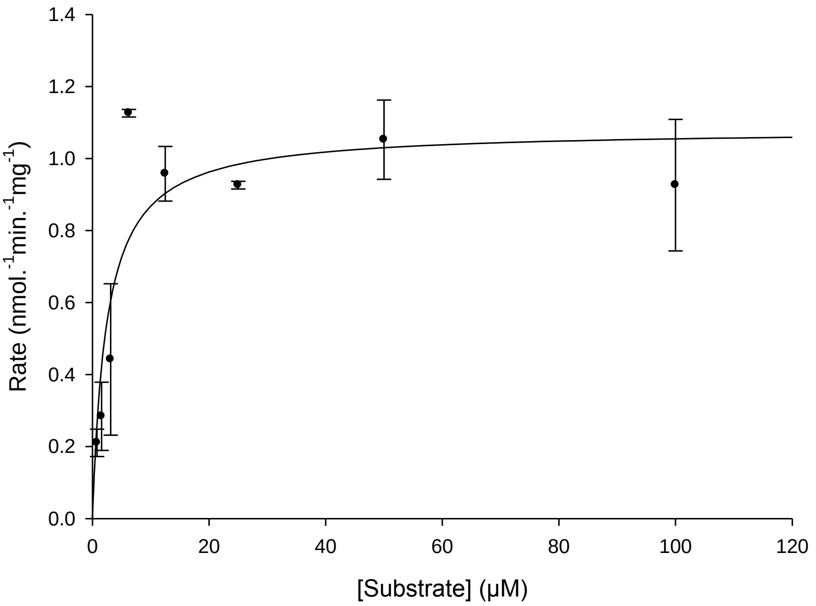

Parameters

	Value	±Std. Error	95% Conf. Interval		
V_{max}	1.0804	8.920e-2	0.8949	to	1.2659
K_m	2.4503	0.9447	0.4857	to	4.4149

Goodness of Fit

Degrees of Freedom	21
AICc	-61.393
R^2	0.637
Sum of Squares	1.162
Sy.x	0.235
Runs Test p Value	0.447

Data

Number of x values	8
Number of replicates	3
Total number of values	23
Number of missing values	1

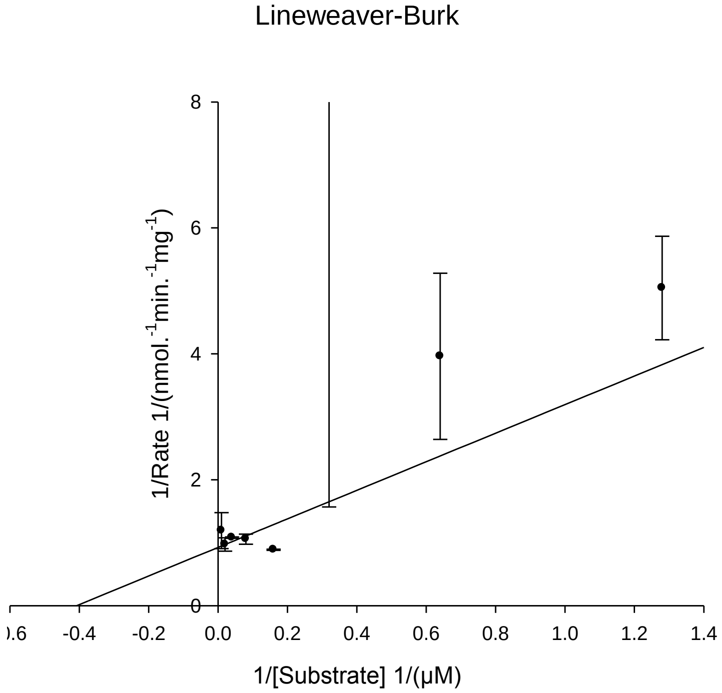
Lineweaver-Burk
1/Rate 1/(nmol.-1min.-1mg-1)
1/[Substrate] 1/(µM)
0
2
4
6
8
-0.4
-0.2
0.0
0.2
0.4
0.6
0.8
1.0
1.2
1.4

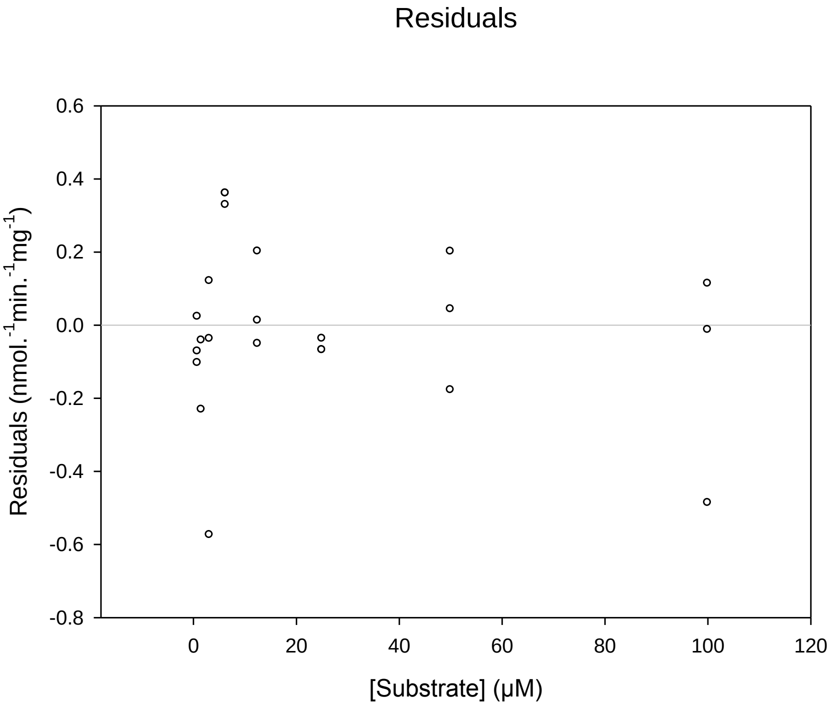
Residuals
Residuals (nmol.-1min.-1mg-1)
[Substrate] (µM)
0.6
0.4
0.2
0.0
-0.2
-0.4
-0.6
-0.8
0
20
40
60
80
100
120

S-2-Methylmyristoyl-CoA 4*S*, ACOT-2

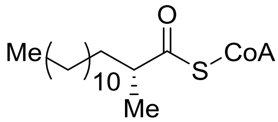

Direct Linear Plot

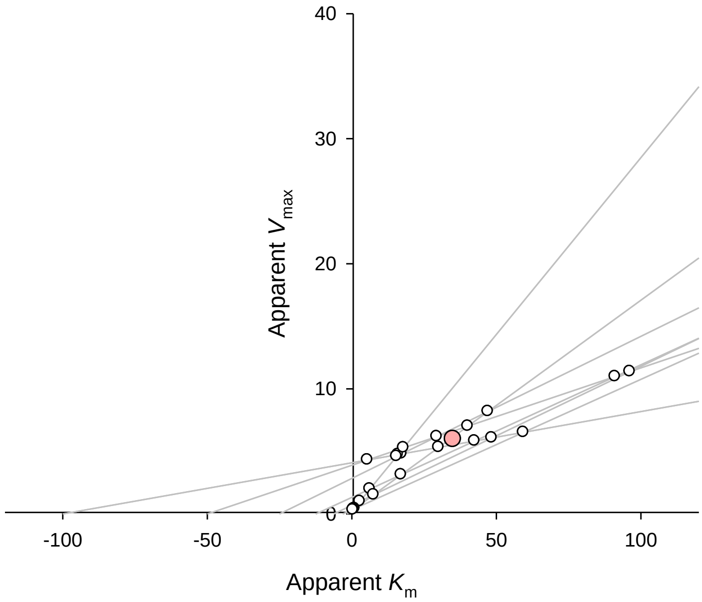

Michaelis-Menten

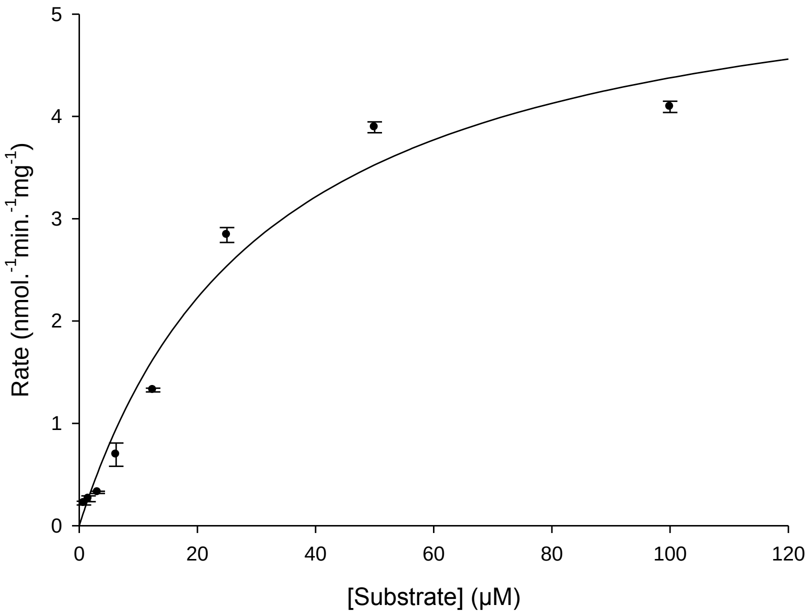

Parameters

	Value	±Std. Error	95% Conf. Interval		
V_{max}	5.7688	0.3536	5.0354	to	6.5022
K_m	31.7988	4.6683	22.1171	to	41.4805

Goodness of Fit

Degrees of Freedom	22
AICc	-56.794
R^2	0.971
Sum of Squares	1.668
Sy.x	0.275
Runs Test p Value	0.387

Data

Number of x values	8
Number of replicates	3
Total number of values	24
Number of missing values	0

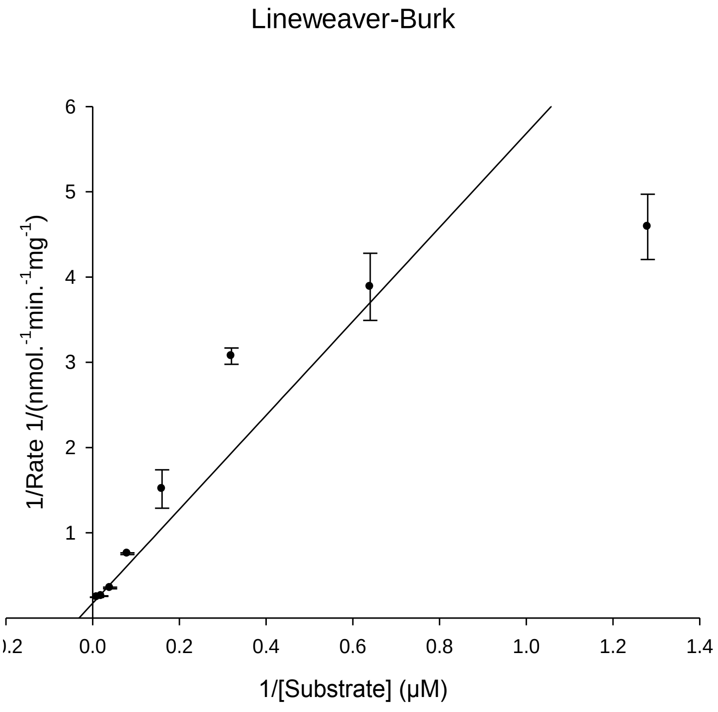

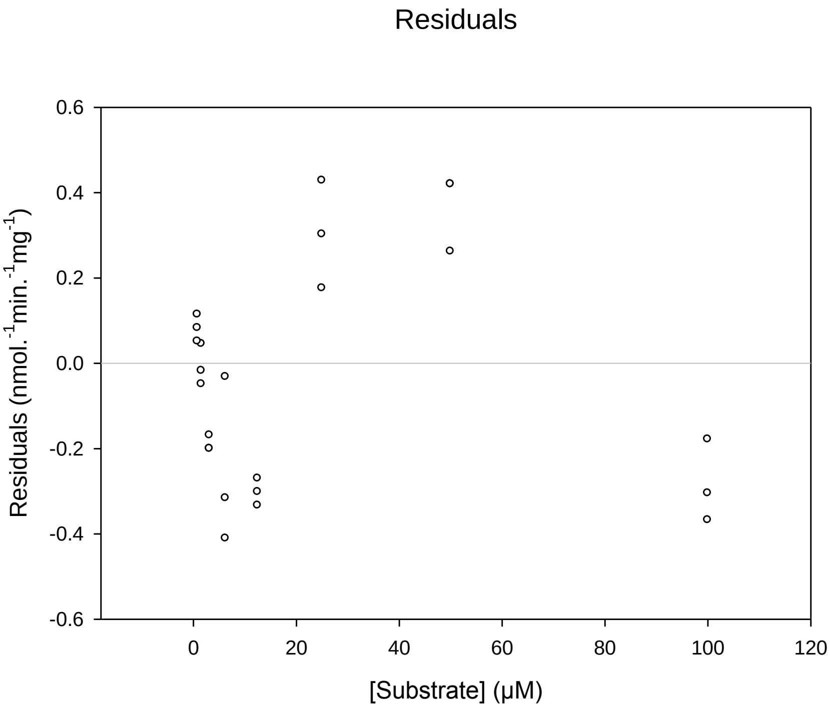

±-Fenoprofenoyl-CoA 5, ACOT-2

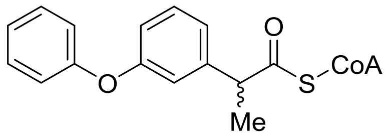

Direct Linear Plot

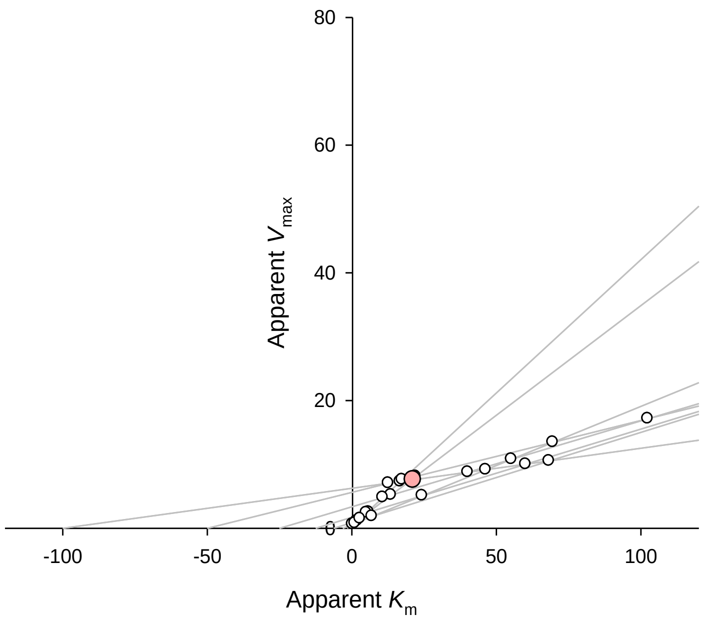

Michaelis-Menten

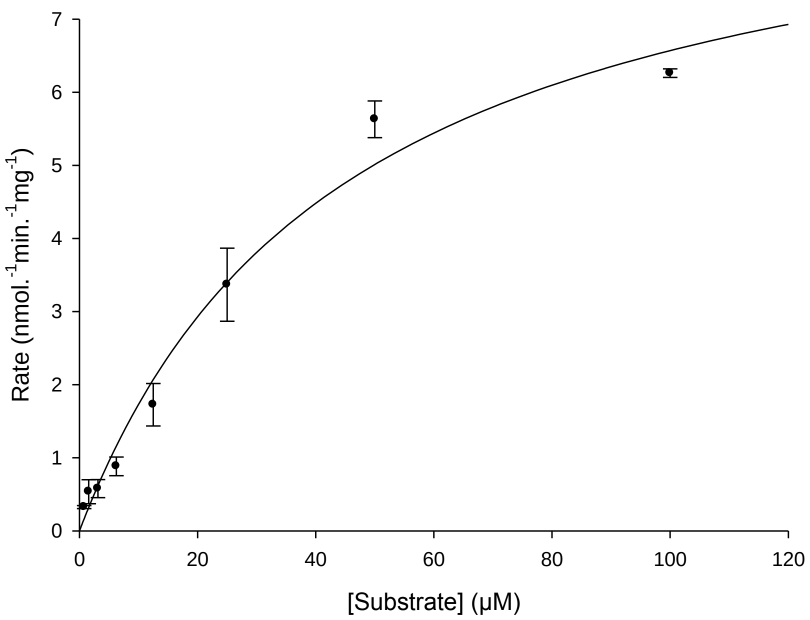

Parameters

	Value	±Std. Error	95% Conf. Interval		
V_{max}	9.5307	0.8409	7.7867	to	11.2747
K_m	45.0815	8.5257	27.3998	to	62.7631

Goodness of Fit

Degrees of Freedom	22
AICc	-30.431
R^2	0.959
Sum of Squares	5.003
Sy.x	0.477
Runs Test p Value	0.350

Data

Number of x values	8
Number of replicates	3
Total number of values	24
Number of missing values	0

Lineweaver-Burk

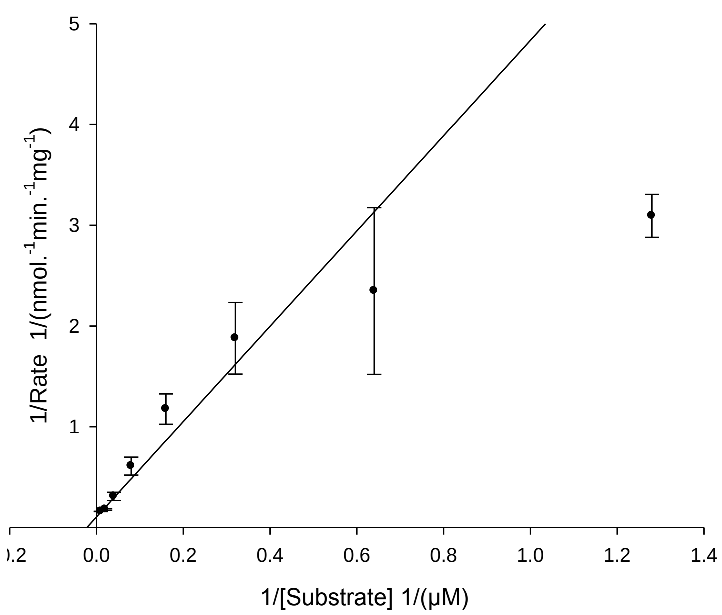

Residuals

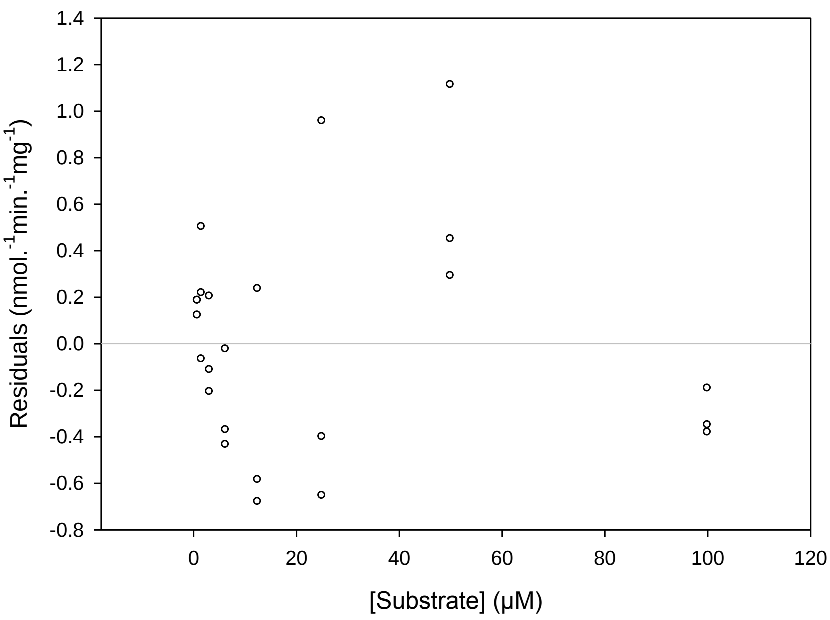

±-Flurbiprofenoyl-CoA 6, ACOT-2

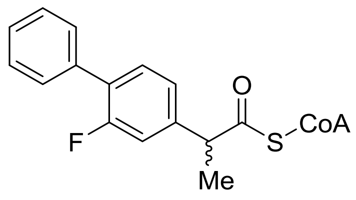

Direct Linear Plot

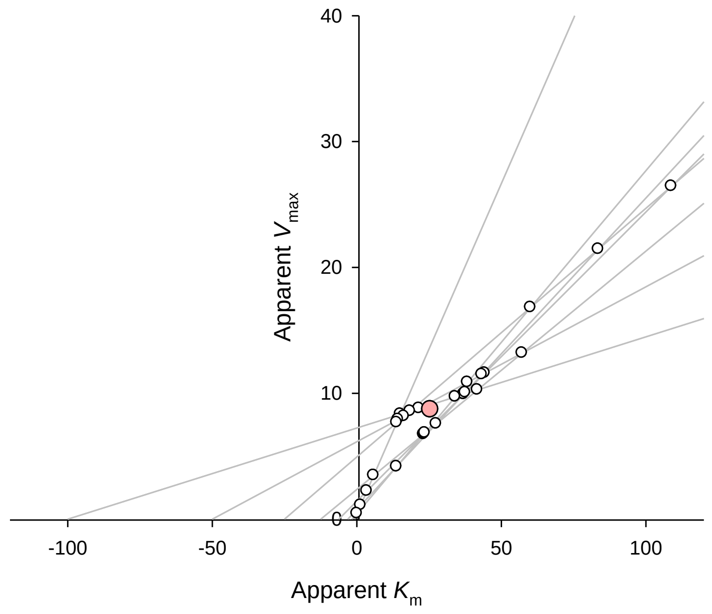

Michaelis-Menten

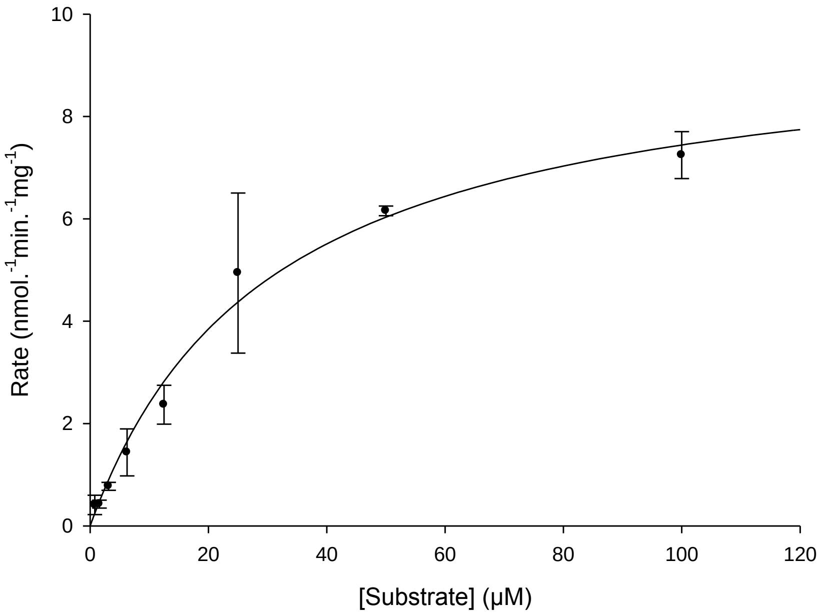

Parameters

	Value	±Std. Error	95% Conf. Interval		
V_{max}	9.7130	1.1102	7.3319	to	12.0941
K_m	30.5008	8.4578	12.3604	to	48.6413

Goodness of Fit

Degrees of Freedom	14
AICc	-4.180
R^2	0.933
Sum of Squares	7.474
Sy.x	0.731
Runs Test p Value	0.277

Data

Number of x values	8
Number of replicates	2
Total number of values	16
Number of missing values	0

Lineweaver-Burk

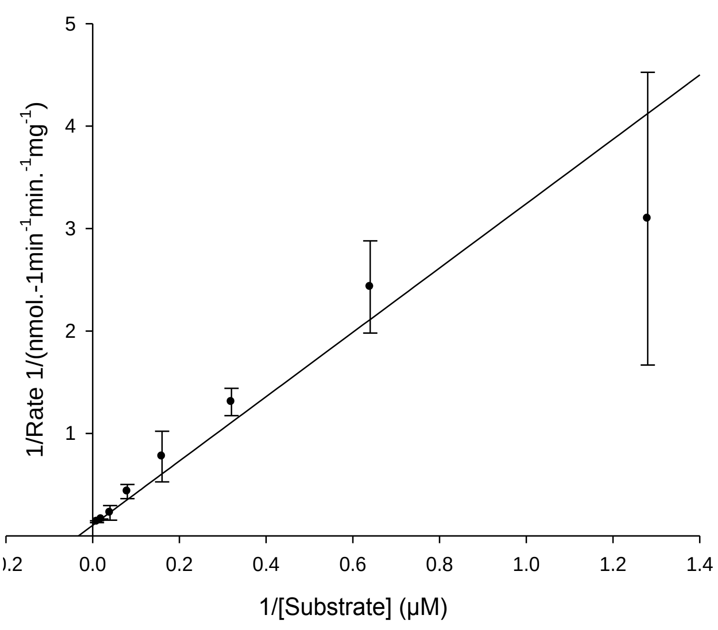

Residuals

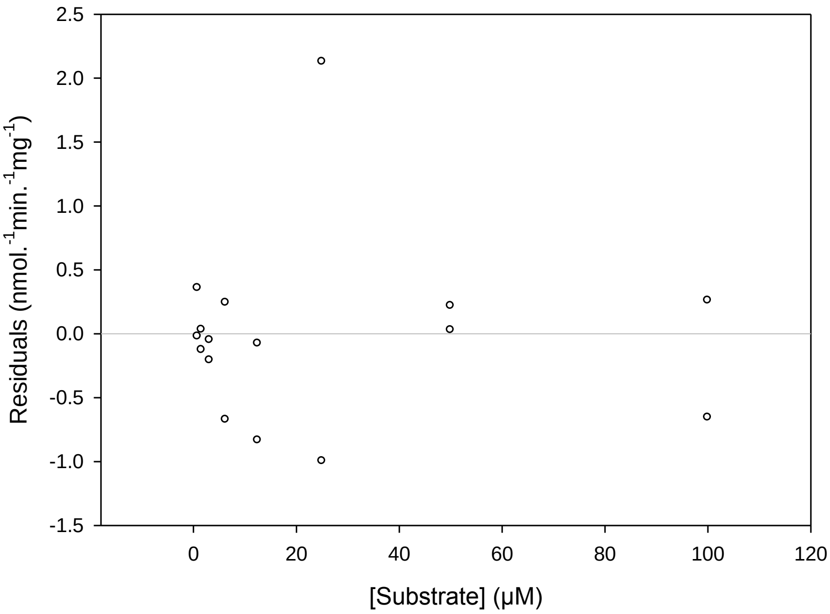

±-Ibuprofenoyl-CoA 2, ACOT-2

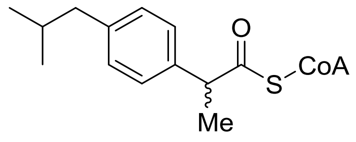

Direct Linear Plot

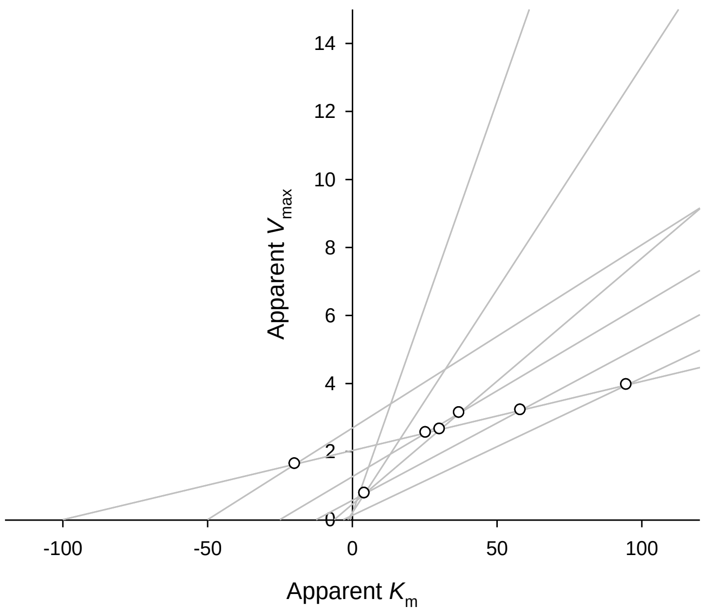

Michaelis-Menten

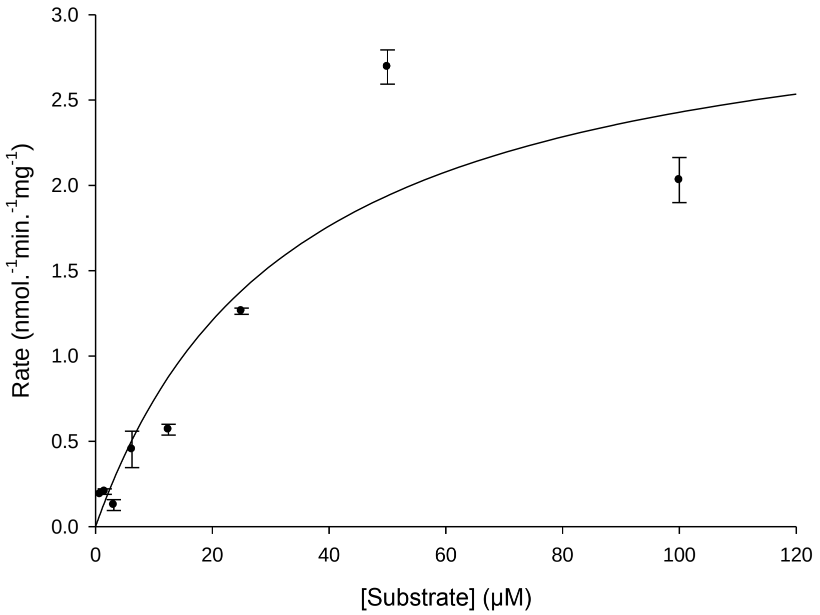

Parameters

	Value	±Std. Error	95% Conf. Interval		
V_{max}	3.2478	0.5254	2.1481	to	4.3475
K_m	33.7370	12.8536	6.8336	to	60.6403

Goodness of Fit

Degrees of Freedom	19
AICc	-34.474
R^2	0.840
Sum of Squares	2.858
Sy.x	0.388
Runs Test p Value	0.199

Data

Number of x values	8
Number of replicates	3
Total number of values	21
Number of missing values	3

Lineweaver-Burk

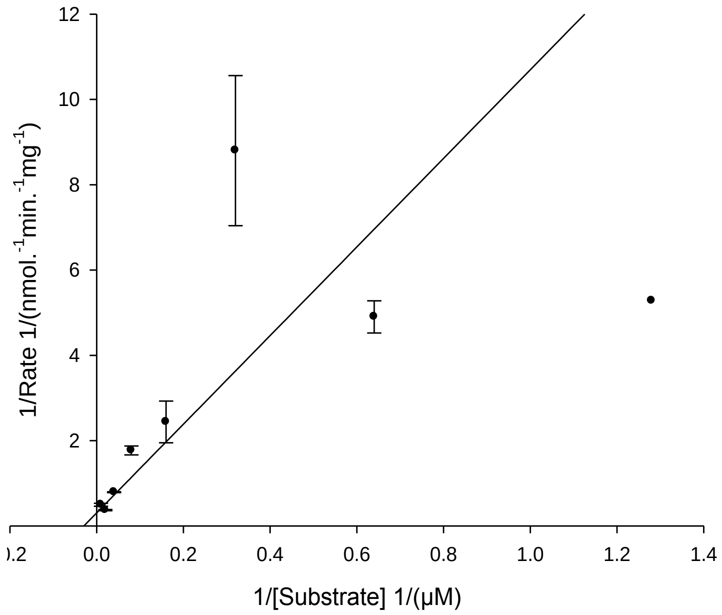

Residuals

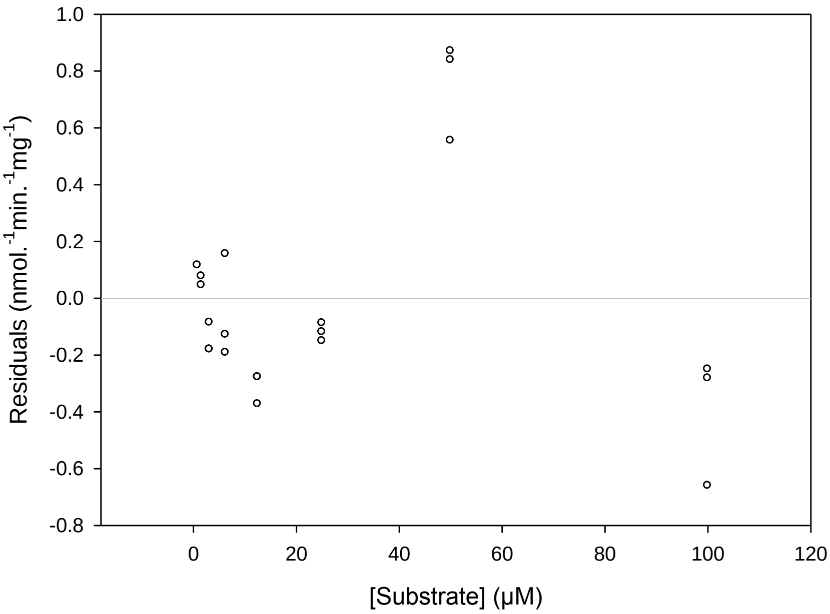

S-Ketoprofenoyl-CoA 7, ACOT-2

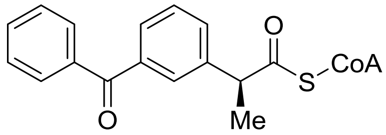

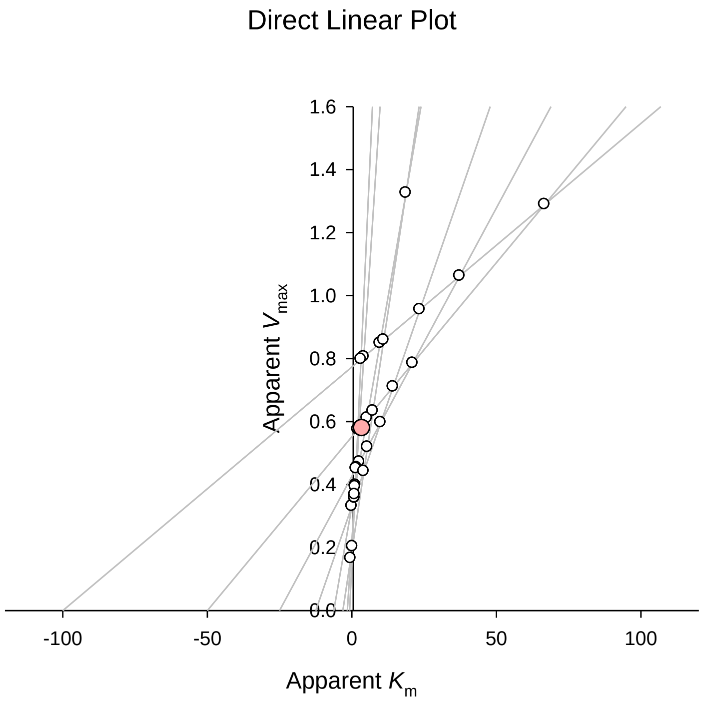

Michaelis-Menten

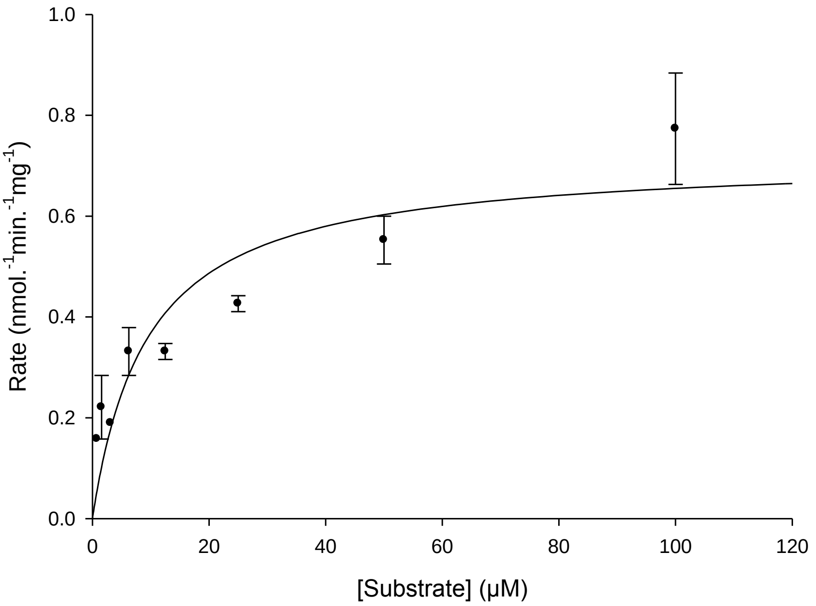

Parameters

	Value	±Std. Error	95% Conf. Interval		
V_{max}	0.7170	7.780e-2	0.5502	to	0.8839
K_m	9.4655	3.4336	2.1011	to	16.8299

Goodness of Fit

Degrees of Freedom	14
AICc	-65.768
R^2	0.754
Sum of Squares	0.159
Sy.x	0.107
Runs Test p Value	0.501

Data

Number of x values	8
Number of replicates	2
Total number of values	16
Number of missing values	0

Lineweaver-Burk

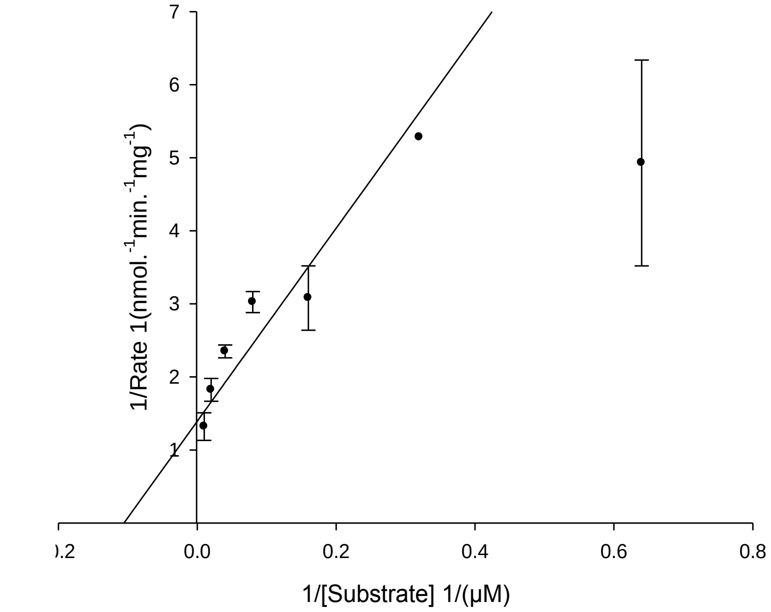

Residuals

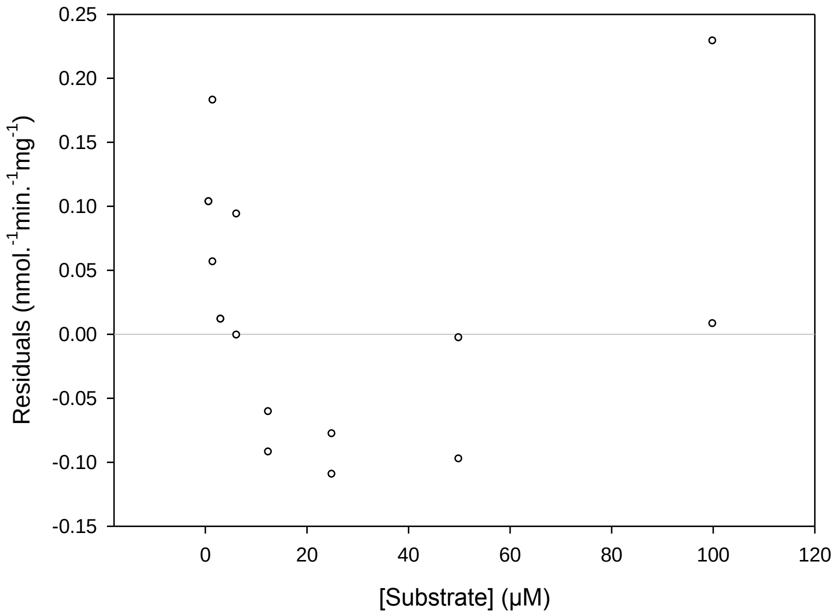

_S_-Naproxenoyl-CoA 8, ACOT-2

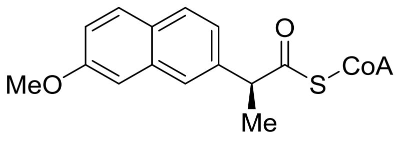

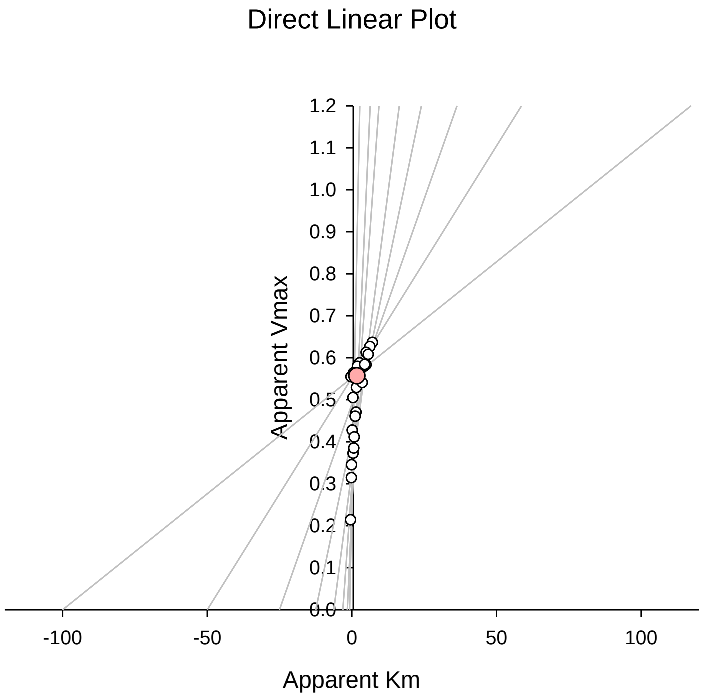

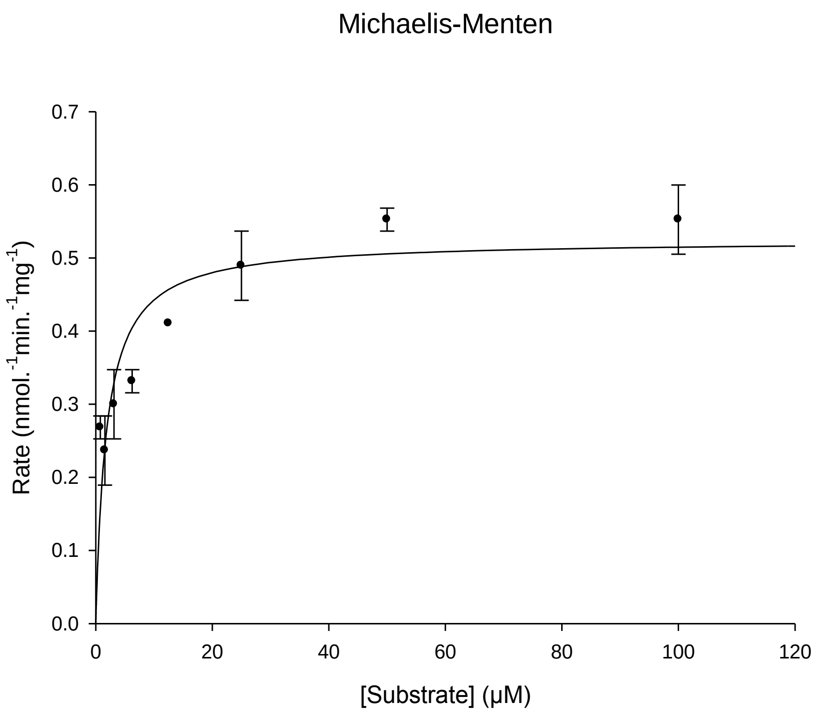

Parameters

	Value	±Std. Error	95% Conf. Interval		
V_{max}	0.5242	3.025e-2	0.4593	to	0.5891
K_m	1.8480	0.5116	0.7506	to	2.9453

Goodness of Fit

Degrees of Freedom	14
AICc	-79.194
R^2	0.720
Sum of Squares	6.876e-2
Sy.x	7.008e-2
Runs Test p Value	0.060

Data

Number of x values	8
Number of replicates	2
Total number of values	16
Number of missing values	0

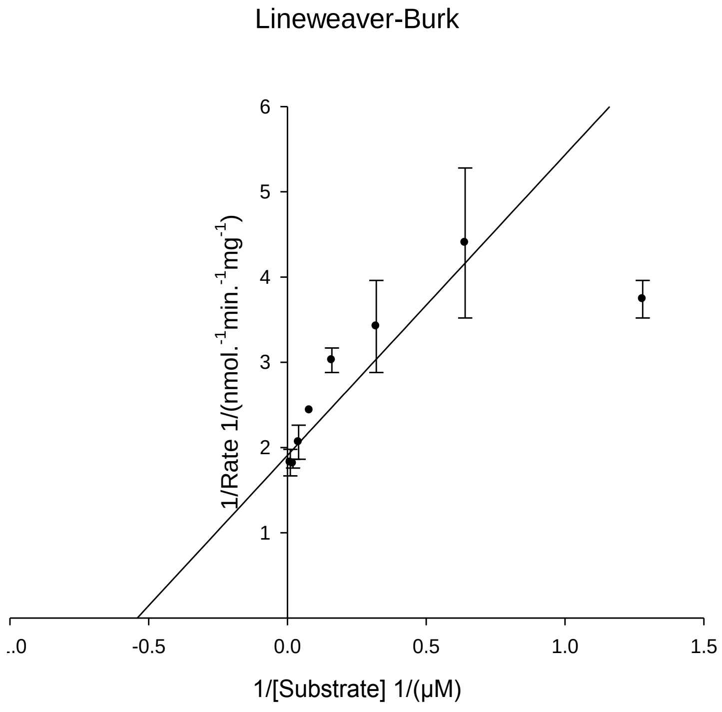
Lineweaver-Burk
1/Rate 1/(nmol.-1min.-1mg-1)
1/[Substrate] 1/(µM)
..0
-0.5
0.0
0.5
1.0
1.5
1
2
3
4
5
6

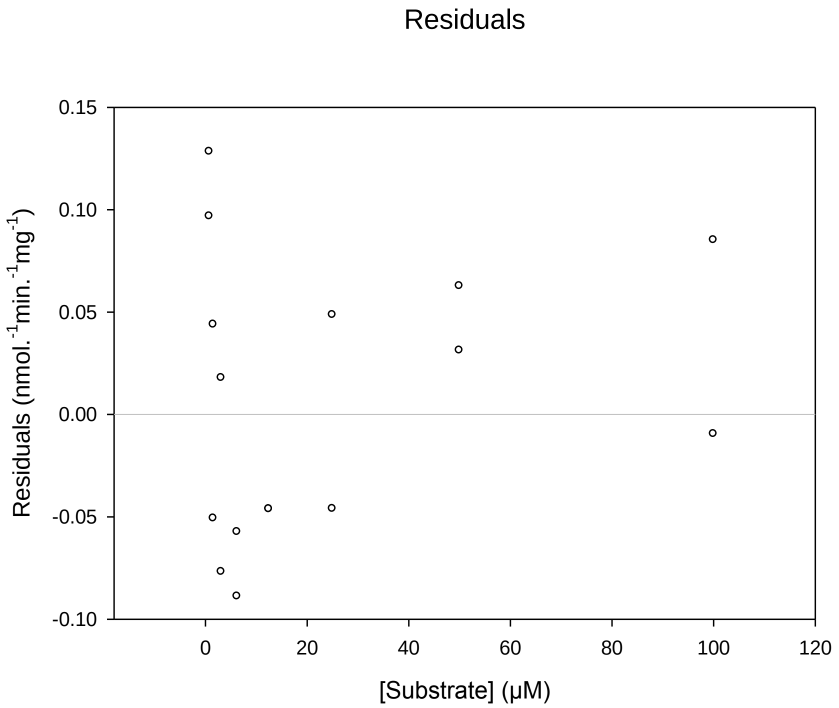
Residuals
Residuals (nmol.-1min.-1mg-1)
[Substrate] (µM)
0.15
0.10
0.05
0.00
-0.05
-0.10
0
20
40
60
80
100
120

Figure S1: Sequence alignment of human ACOT-1 and ACOT-2

```
ACOT-1        ------------------------------------------------------------
ACOT-2        MSNKLLSPHPHSVVLRSEFKMASSPAVLRASRLYQWSLKSSAQFLGSPQLRQVGQIIRVP

ACOT-1        --MAATLILEPAGRCCWDEPVRIAVRGLAPEQPVTLRASLRDEKGALFQAHARYRADTLG
ACOT-2        ARMAATLILEPAGRCCWDEPVRIAVRGLAPEQPVTLRASLRDEKGALFQAHARYRADTLG
                **********************************************************

ACOT-1        ELDLERAPALGGSFAGLEPMGLLWALEPEKPLVRLVKRDVRTPLAVELEVLDGHDPDPGR
ACOT-2        ELDLERAPALGGSFAGLEPMGLLWALEPEKPLVRLVKRDVRTPLAVELEVLDGHDPDPGR
              ************************************************************

ACOT-1        LLCRVRHERYFLPPGVRREPVRAGRVRGTLFLPPEPGPFPGIVDMFGTGGGLLEYRASLL
ACOT-2        LLCQTRHERYFLPPGVRREPVRVGRVRGTLFLPPEPGPFPGIVDMFGTGGGLLEYRASLL
              ***:.*****************.*************************************

ACOT-1        AGKGFAVMALAYYNYEDLPKTMETLHLEYFEEAVNYLLSHPEVKGPGVGLLGISKGGELC
ACOT-2        AGKGFAVMALAYYNYEDLPKTMETLHLEYFEEAMNYLLSHPEVKGPGVGLLGISKGGELC
              *********************************:**************************

ACOT-1        LSMASFLKGITAAVVINGSVANVGGTLRYKGETLPPVGVNRNRIKVTKDGYADIVDVLNS
ACOT-2        LSMASFLKGITAAVVINGSVANVGGTLRYKGETLPPVGVNRNRIKVTKDGYADIVDVLNS
              ************************************************************

ACOT-1        PLEGPDQKSFIPVERAESTFLFLVGQDDHNWKSEFYANEACKRLQAHGRRKPQIICYPET
ACOT-2        PLEGPDQKSFIPVERAESTFLFLVGQDDHNWKSEFYANEACKRLQAHGRRKPQIICYPET
              ************************************************************

ACOT-1        GHYIEPPYFPLCRASLHALVGSPIIWGGEPRAHAMAQVDAWKQLQTFFHKHLGGREGTIP
ACOT-2        GHYIEPPYFPLCRASLHALVGSPIIWGGEPRAHAMAQVDAWKQLQTFFHKHLGGHEGTIP
              ******************************************************:*****

ACOT-1        SKV
ACOT-2        SKV
              ***
```

Figure S1: Primary sequence alignment of human ACOT-1 (A1L172) and ACOT-2 (P49753). Sequences were obtained from http://www.uniprot.org/ and aligned with ClusterW (http://www.ch.embnet.org/software/ClustalW.html) with default parameters. Active site catalytic triad residues are shown in green.